https://doi.org/10.5194/egusphere-2026-3480
Preprint. Discussion started: 25 June 2026

Analysis of inorganic chlorine chemistry in the midlatitude summer stratosphere using aircraft and satellite observations

David M. Wilmouth[1], Jennifer S. Hare[1], Laila V. Howar[2], Ross J. Salawitch[2], Eric J. Hintsa[3,4], Jessica B. Smith[1], David S. Sayres[1], James G. Anderson[1], Jason M. St. Clair[5,6], Erin R. Delaria[2,5], Reem A. Hannun[7], Thomas F. Hanisco[5], Daniel J. Czizco[8,9], Xiaoli Shen[8,10], Cameron R. Homeyer[11], Michelle L. Santee[12], T. Paul Bui[7,13], Paul A. Newman[5,6], Frank N. Keutsch[1], and Kenneth P. Bowman[14]

[1]Harvard University, Cambridge, MA, USA; [2]University of Maryland, College Park, MD, USA; [3]Cooperative Institute for Research in Environmental Sciences, University of Colorado Boulder, Boulder, CO, USA; [4]NOAA Global Monitoring Laboratory, Boulder, CO, USA; [5]NASA Goddard Space Flight Center, Greenbelt, MD, USA; [6]University of Maryland, Baltimore County, Baltimore, MD, USA; [7]NASA Ames Research Center, Moffett Field, CA, USA; [8]Purdue University, West Lafayette, IN, USA; [9]University of Chicago, Chicago, IL, USA; [10]Institute of Meteorology and Climate Research, Karlsruhe Institute of Technology, Eggenstein-Leopoldshafen, Germany; [11]University of Oklahoma, Norman, OK, USA; [12]Jet Propulsion Laboratory, California Institute of Technology, Pasadena, CA, USA; [13]Bay Area Environmental Research Institute, Moffett Field, CA, USA; [14]Texas A&M University, College Station, TX, USA

Correspondence: David M. Wilmouth (wilmouth@huarp.harvard.edu)

Abstract. In recent years, significant perturbations to stratospheric inorganic chlorine have been observed following wildfires or volcanic eruptions, as well as modeled in simulations with elevated water vapor from overshooting convection or organic species in biomass burning aerosol. A detailed evaluation of inorganic chlorine in the stratosphere sampled under various conditions is presented here using high precision in situ aircraft measurements of chlorine monoxide (ClO) and chlorine nitrate ($ClONO_2$). Data were obtained over North America during the NASA Dynamics and Chemistry of the Summer Stratosphere (DCOTSS) mission. The vertical distributions of ClO and $ClONO_2$ from all 29 research flights of the 2-year mission are found to be relatively compact and lacking substantial outliers. The peak mixing ratios are approximately 30 ppt and 400 ppt for ClO and $ClONO_2$, respectively. No chlorine activation was observed in the lower stratosphere in the presence of low temperatures and elevated water vapor from convective injection. Steady-state calculated $ClONO_2$ is found to be in good agreement with measured values, suggesting that a reduction in the uncertainty of the recommended rate coefficient for $ClONO_2$ production is possible. HCl is calculated at high time resolution throughout the mission using satellite data, and the resulting evaluation of the inorganic chlorine budget shows excellent agreement, with the ratio of ClO + $ClONO_2$ + HCl to total inorganic chlorine equal to 0.95 for mixing ratios greater than 500 ppt. No evidence of inorganic chlorine activation was observed during DCOTSS when aerosol organic mass fraction and biomass burning fraction were elevated.

https://doi.org/10.5194/egusphere-2026-3480
Preprint. Discussion started: 25 June 2026

1 Introduction

Extraordinary perturbations to Earth's stratospheric composition have occurred in just the past few years. These significant and unforeseen changes to stratospheric constituents have in some cases exposed gaps in our understanding and highlighted the need for ongoing study of stratospheric chemical and dynamical processes (Salawitch et al., 2025). For example, the Australian New Year's (ANY) fires in 2019-2020 led to substantial changes in inorganic chlorine concentrations in the midlatitude stratosphere (Santee et al., 2022; Strahan et al., 2022; Salawitch and McBride, 2022; Solomon et al., 2023; Chipperfield and Bekki, 2024), with previously unconsidered heterogeneous chemistry on organic aerosols appearing to be the likely cause (Solomon et al., 2023; Stone et al., 2025). The Hunga volcanic eruption in 2022 caused extraordinary enhancements in stratospheric water vapor with more modest increases in sulfate and led to large changes in inorganic chlorine partitioning, ozone, and other compounds in the stratosphere (Millán et al., 2022; Santee et al., 2023; Wilmouth et al., 2023). In 2023, a serendipitous discovery was made that metals vaporized upon spacecraft reentry to Earth are now observable in sulfuric acid particles in the stratosphere (Murphy et al., 2023). Given the rapid growth in the space industry, there will likely be orders of magnitude increases in space debris in the stratosphere, with unknown potential impacts on stratospheric chemistry (Murphy et al., 2023; Revell et al., 2025).

Against this backdrop of ongoing change, it is important to evaluate our understanding of stratospheric chlorine chemistry, as chemical cycles involving inorganic chlorine exert significant control on Earth's protective ozone layer. The recent NASA Earth Venture Suborbital (EVS-3) campaign—Dynamics and Chemistry of the Summer Stratosphere (DCOTSS)—provided this opportunity, with 29 research flights in summers 2021 and 2022 over North America (Bowman et al., 2026). The Harvard Halogens (HAL) instrument made highly sensitive in situ measurements of chlorine monoxide (ClO) and chlorine nitrate ($ClONO_2$) from the ER-2 aircraft throughout the campaign. In addition to examining inorganic chlorine chemistry in the background stratosphere, the DCOTSS mission also provided the first opportunity to test, using in situ measurements, the possibility of heterogeneous chlorine activation and subsequent ozone loss occurring over North America in summertime. As shown by several modeling studies (Anderson et al., 2012; Anderson et al., 2017; Robrecht et al., 2019), this chemistry could become significant under conditions of low temperature and elevated water vapor found in the lower stratosphere following tropopause-overshooting convective injection, which is frequent in the North American Monsoon Anticyclone (NAMA) region.

For the past two decades, the atmospheric sciences community has benefited immeasurably from continuous daily satellite measurements of the inorganic halogens ClO and HCl (hydrogen chloride) from the Microwave Limb Sounder (MLS) instrument on Aura, as well as the Atmospheric Chemistry Experiment–Fourier Transform Spectrometer (ACE-FTS) satellite instrument on SCISAT-1, which also measures $ClONO_2$. The in situ chlorine measurements from HAL during DCOTSS complement these satellite data and also provide an improved capability, in combination with other concurrent aircraft measurements, to test our understanding of chlorine photochemistry and kinetics due to the superior precision of the in situ data and targeted aircraft sampling. The DCOTSS mission addresses a surprising void in the in situ record in which the chemistry of the stratosphere over the contiguous United States in summertime has been relatively undersampled.

https://doi.org/10.5194/egusphere-2026-3480
Preprint. Discussion started: 25 June 2026

In this study, we analyze the stratospheric in situ chemical data from the DCOTSS mission to establish the dominant factor controlling inorganic chlorine mixing ratios, to explore the possibility of heterogeneous chlorine activation in stratospheric air influenced by tropopause-overshooting convection, and to quantitatively test the established photochemistry and kinetics of $ClONO_2$ formation and loss. We further calculate HCl for the time and location of aircraft sampling using a technique that combines satellite and in situ data. This calculated HCl is used with measured ClO, measured $ClONO_2$, and calculated total inorganic chlorine to test closure of the inorganic chlorine budget in the stratosphere. In situ data are compared with relevant satellite data throughout the analysis.

Anthropogenic climate disruption has resulted in an unprecedented increase in wildfire frequency and intensity globally, with pyroconvection from these severe wildfires potentially injecting biomass burning products into the lower stratosphere, increasing aerosol loading and altering stratospheric composition (Ellis et al., 2022; Fromm et al., 2022; Ansmann et al., 2022). In this study, we look for observational evidence from DCOTSS of the heterogeneous chlorine chemistry mechanism that was identified by Solomon et al. (2023) as being responsible for elevated ClO and $ClONO_2$ mixing ratios following the ANY fires, in which the presence of enhanced organic aerosol led to heterogeneous uptake of HCl at relatively warm temperatures.

2 Experimental

All in situ data analyzed in this study were obtained from instruments flown onboard the high-altitude ER-2 aircraft during the NASA DCOTSS mission based out of Salina, KS and Palmdale, CA. There were 31 total flights in the mission, with 29 of those representing science research flights, which took place in June–August 2021 and May–July 2022. The operational base of Salina, KS in summertime was chosen to optimize sampling of strong convective storms in the NAMA region that regularly penetrate deep into the lower stratosphere (e.g., Anderson et al., 2012; Smith et al., 2017; Cooney et al., 2018; Liu et al., 2020; Homeyer and Bowman, 2021; Homeyer et al., 2023). The primary goals of the DCOTSS project were to improve understanding of the effects of deep convection and large-scale dynamics on the composition and chemistry of the lower stratosphere over North America and to extensively sample the background stratosphere. A detailed overview of the DCOTSS mission, including a description of each ER-2 flight and the instrumentation onboard, was presented by Bowman et al. (2026).

2.1 Inorganic Chlorine Measurements

The HAL instrument uses thermal dissociation / atomic resonance fluorescence detection to make highly sensitive measurements of inorganic halogens at four independent axes. The technique used for measurement of ClO involves chemical titration via a rapid bimolecular reaction with NO, followed by resonance fluorescence detection of the resulting Cl atoms in the vacuum ultraviolet (Anderson et al., 1977; Brune et al., 1989; Anderson et al., 1991; Stimpfle et al., 2004; Wilmouth et al., 2009). Measurement of $ClONO_2$ requires an initial step of rapid thermal dissociation to break the weak ClO–NO_2 bond, followed by detection of the dissociated ClO in the same manner as ambient ClO (Stimpfle et al., 1999; Stimpfle et al., 2004; Wilmouth et al., 2006). Each independent detection axis contains a custom-built resonance fluorescence lamp (Hare et al., 2024), optimized for Cl detection at 118.9 nm, and a photomultiplier

https://doi.org/10.5194/egusphere-2026-3480
Preprint. Discussion started: 25 June 2026

tube detector positioned perpendicular to the lamp. A description of the Harvard Halogens flight instrument, along with a schematic diagram and photo, are included in Fig. S1 and in the accompanying Supplement text.

The instrument was calibrated in the laboratory under pressures and flow velocities typical of flight. The absolute sensitivity of each detection axis in flight was determined at systematic intervals from the observed Rayleigh scatter as a function of air density. The estimated accuracy of the ClO measurement is 17% (all uncertainties reported herein are 1σ) with a precision of 2 ppt (parts per trillion; all reported mixing ratios herein are by volume) in a sampling interval of 35 seconds. The data rate of 35 seconds is set by the timing of the NO titration cycle. The estimated accuracy of the $ClONO_2$ measurement is 20% with a precision of 5 ppt in 35 seconds, with data only being reported when the dissociation heater cycle is at the highest temperatures (~500 K). The detection limit of the HAL instrument with additional data averaging was very low during DCOTSS, with discrimination of approximately 0.2 ppt for ClO and 2 ppt for $ClONO_2$. The measurement precision achieved during the DCOTSS mission for both ClO and $ClONO_2$ was approximately a factor of two higher than previous flight values (Stimpfle et al., 2004) due to improvements in the optical system. The excellent agreement between the ClO data from multiple independent HAL detection axes provides additional confidence in the accuracy of the measurements.

2.2 Other In Situ Data

The ER-2 carried a payload of 12 instruments to measure trace gases, aerosol properties, and meteorology during the DCOTSS flights (Bowman et al., 2026). A complete list of the in situ measurements with specified precision and accuracy appears in Table 1 of Howar et al. (2025). The trace gas measurements used in the present study include: ozone (O_3) from the Rapid Ozone Experiment (ROZE), reported with a precision of 1 ppb and accuracy of 6% (Hannun et al., 2020); nitrogen dioxide (NO_2) from the Compact Airborne Nitrogen dioxide Experiment (CANOE), reported with a precision of 50 ppt and accuracy of 10% (St. Clair et al., 2019); and water vapor (H_2O) from the Harvard Herriott Hygrometer (HHH) as part of the Harvard Water Vapor (HWV) instrument, reported with a precision of 0.1 ppm and accuracy of 5% (Sargent et al., 2013). Temperature (T), pressure (P), and potential temperature (θ) were measured by the Meteorological Measurement System (MMS) with accuracies of 0.3 K, 0.3 hPa, and 0.5–1.5 K, respectively (Scott et al., 1990).

Aerosol fractional composition products were reported by the Particle Analysis by Laser Mass Spectrometry-Next Generation (PALMS-NG) instrument as a value from 0 to 1, with approximate uncertainty of 1–10%. PALMS-NG detects and obtains size information on single particles via light scattering and then determines chemical composition using a one-step Laser Desorption and Ionization technique combined with dual time-of-flight mass spectrometers (Jacquot et al., 2024). This Single Particle Mass Spectrometry technique allows for measurement of refractory and non-refractory particle components over a size range from ~0.1 to 10 micrometer diameter.

Three values that were not measured are calculated for all flights of the mission: (a) HCl was determined using a combination of satellite and in situ data, as discussed in detail in Section 3.5. (b) Total inorganic chlorine (Cl_y) was determined by Howar et al. (2025) as the difference between organic chlorine measured in the stratosphere during DCOTSS by the Advanced Whole Air Sampler (Smith et al., 2024) and the total organic chlorine burden in the troposphere at the time of stratospheric entry. We use the average of the Howar et al. (2025) upper and lower limit

https://doi.org/10.5194/egusphere-2026-3480
Preprint. Discussion started: 25 June 2026

estimates of Cl_y, which include both long-lived and Very Short-Lived (VSL) chlorine species. This analysis provides total inorganic chlorine with an approximate uncertainty of 6% when $Cl_y > 500$ ppt, with larger uncertainties at smaller mixing ratios, as discussed in Section 3.5. (c) Photolysis rates for $ClONO_2$ (J_{ClONO2}) were calculated using a radiative transfer model that accounts for Rayleigh scattering (Salawitch et al., 1994) constrained by surface reflectivity from the TROPOspheric Monitoring Instrument (TROPOMI) and vertical profiles of O_3 derived from a combination of ozonesonde and MLS retrievals with total column measurements from TROPOMI, as described by Howar et al. (2025). The absorption cross sections for $ClONO_2$ are taken from the NASA JPL-19 recommendation (Burkholder et al., 2019). The estimated uncertainty in J_{ClONO2} values used here is 10%.

2.3 Satellite Data

MLS measurements of HCl, O_3, and ClO are used in this study, as are ACE-FTS (hereafter, ACE) measurements of $ClONO_2$ and ClO. MLS measures microwave thermal emission from the limb of Earth's atmosphere to obtain vertical profiles of trace gases at various pressure levels with daily global coverage. MLS Version 5, Level 2 data are used. All data screening recommendations from the MLS Version 5 Data Quality document (Livesey et al., 2022) were applied to each variable. For HCl, the individual-profile precision / accuracy are estimated to be 300 ppt / 100 ppt, 200 ppt / 100 ppt, and 200 ppt / 100 ppt at 100, 68, and 46 hPa, respectively, and the vertical resolution is 3 km over that range. For O_3, the individual-profile precision / accuracy are estimated to be 40 ppb / (+2.5 ppb + 4%), 40 ppb / 50 ppb, and 60 ppb / 100 ppb at 100, 68, and 46 hPa, respectively, and the vertical resolution is 2.5 km over that range. For ClO, the individual-profile precision and vertical resolution are estimated to be 100 ppt and 3 km, respectively, over the 100 to 46 hPa pressure range. The ClO measurement has known biases at the 100 and 68 hPa retrieval pressure levels, and the appropriate MLS-recommended bias corrections (Livesey et al., 2022) were implemented.

ACE measures $ClONO_2$ and ClO using Fourier Transform infrared spectroscopy at sunrise and sunset. ACE has relatively sparse observational coverage outside of the high latitudes, and ClO is a very weak absorber, which makes it difficult to measure when ClO concentrations are not elevated as in chlorine processing events in polar spring. To our knowledge, pressure-dependent precision and accuracy data comparable to those listed for MLS measurements are not available for ACE measurements. The version 5.2 data used here were filtered for outliers beyond 3 standard deviations from the mean in accordance with the ACE team recommendations, where appropriate (Boone et al., 2023).

3 Results and Discussion

3.1 Inorganic Chlorine

The DCOTSS mission extensively sampled the stratosphere over much of the contiguous United States, as well as north into Canada and over the Pacific Ocean off the west coasts of the US and Mexico. Example flight data are shown for the DCOTSS flight of 16 July 2021 in Fig. 1. The primary objective of this flight was to survey the Northern Hemisphere midlatitude summer stratosphere. On this 8-hour flight, the ER-2 took off at 14:13 UT (9:13 AM CDT) from Salina, KS, flew southeast to southern IL, then turned north, flying up to Hudson Bay, Canada, then back to Salina, KS. Potential temperature and solar zenith angle (SZA) for the flight are shown in Fig. 1a, with mixing ratios

https://doi.org/10.5194/egusphere-2026-3480
Preprint. Discussion started: 25 June 2026

of ClO and $ClONO_2$ as a function of flight time plotted in Figs. 1b and 1c, respectively. The vertical coordinate is shown as potential temperature rather than altitude because, in the absence of diabatic processes, air parcels in the stratosphere are transported along surfaces of constant potential temperature. There were many level flight legs in the first half of the flight, of approximately 20-minute duration, followed by several extensive vertical profiles in the second half. The peak altitudes reached by the ER-2 represented by the maximum potential temperatures shown in Fig. 1 were approximately 20.5 – 21.1 km above mean sea level. Other than takeoff, landing, and the deepest descents, the flight was dominated by stratospheric air, evidenced by ozone mixing ratios exceeding 200 ppb with water mixing ratios below 6 ppm (not shown).

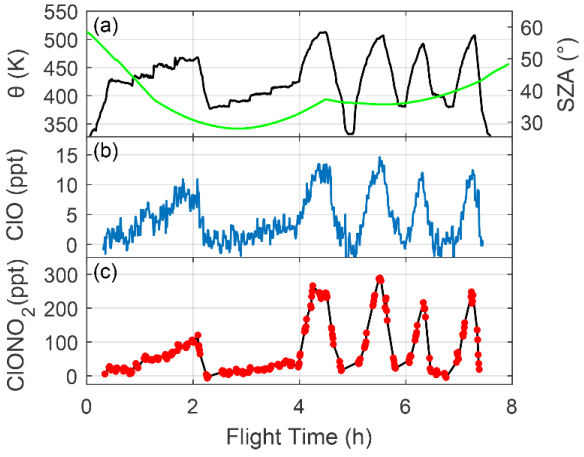

Figure 1. In situ measurements from the DCOTSS flight on 16 July 2021 over North America on the NASA ER-2. (a) Potential temperature (black) as measured by MMS and solar zenith angle (green). Mixing ratios of (b) ClO and (c) $ClONO_2$ as measured by HAL in units of parts per trillion by volume. The black line in panel (c) connects the measured points to guide the eye.

Strong correlations between the inorganic chlorine species and potential temperature are evident in Fig. 1. Mixing ratios of ClO and $ClONO_2$ slowly increase as θ gradually rises across the level flight legs in the first half of the flight, then mixing ratios more rapidly increase and decrease in concert with the vertical profiles in θ during the second half of the flight. The peak ClO and $ClONO_2$ mixing ratios observed on this flight were approximately 15 ppt and 300 ppt, respectively. The red points in Fig. 1c represent the $ClONO_2$ measurements, which as indicated earlier, are less frequent than the other observations shown due to the required synchronization of the HAL NO titration cycle and dissociation heater cycle. As shown by the solar zenith angle in Fig. 1a, this entire survey flight was during daylight hours, so the vertical structure in ClO and $ClONO_2$ mixing ratios was unaffected by nighttime impacts to photochemistry.

To extend this analysis across the entire mission, Fig. 2 shows potential temperature versus mixing ratio of ClO and $ClONO_2$ in panels 2a and 2b, respectively, for all 29 DCOTSS research flights. The vertical axis includes measurements obtained in the upper troposphere up through and including all stratospheric measurements from the

https://doi.org/10.5194/egusphere-2026-3480
Preprint. Discussion started: 25 June 2026

mission, reaching potential temperatures up to approximately 520 K. The highest sampling altitude achieved by the ER-2 during the DCOTSS mission was ~21.3 km. Supplement Fig. S2 provides a useful reference to aid in comparison of DCOTSS data over a variety of vertical coordinates, displaying pressure, potential temperature, and ozone versus altitude. Because ClO decreases to zero at night, we separate daytime and nighttime data, with the ClO mixing ratios color coded in Fig. 2 based on the solar zenith angle at the time of measurement. Specifically, a threshold of 75º and below is used to represent daytime ClO in Fig. 2a and in subsequent figures of this work (although the exact threshold SZA used is not critical). Approximately 91% of the ClO data as represented in Fig. 2 are categorized as daytime values.

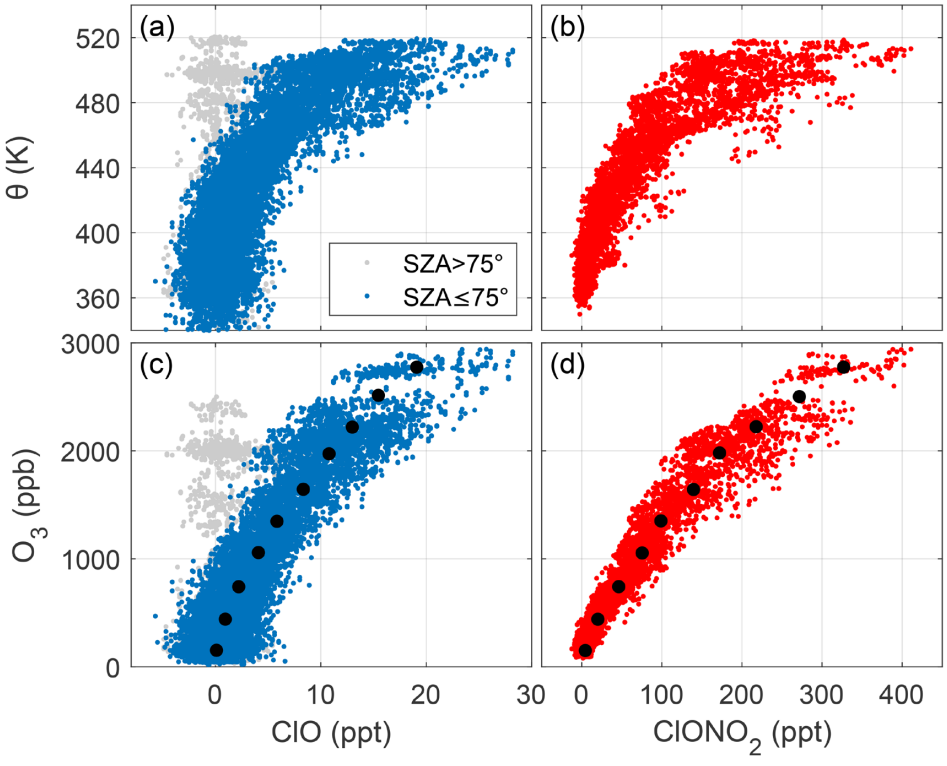

Figure 2. Measurements of ClO and $ClONO_2$ as a function of (a), (b) potential temperature and (c), (d) ozone, respectively, for all 29 research flights of the NASA DCOTSS mission. ClO data are color-coded based on the solar zenith angle at the time of measurement: blue indicates SZA at or below 75˚ (daytime), and gray indicates SZA greater than 75˚. All $ClONO_2$ data from the mission are in red. The larger black circles in (c) and (d) are averages of ClO and $ClONO_2$, respectively, in 300 ppb O_3 bins. The number of data points plotted is 16369 for ClO (14845 in blue, 1524 in gray) and 5129 for $ClONO_2$.

Mixing ratios of ClO and $ClONO_2$ increase with increasing potential temperature (Figs. 2a and 2b), rising more slowly in the lowest portion of the stratosphere and subsequently increasing more rapidly and generally with greater variability at θ values above ~460 K. The observed correlation between inorganic chlorine mixing ratios and potential temperature arises because both generally increase with age of air in the midlatitude stratosphere. Nearly all chlorine

https://doi.org/10.5194/egusphere-2026-3480
Preprint. Discussion started: 25 June 2026

enters the stratosphere in organic form in the tropics in the rising part of the Brewer-Dobson circulation and is slowly converted to inorganic form as the air parcel ages during its transit through the stratosphere. Higher values of inorganic chlorine at a given potential temperature in DCOTSS indicate a larger fraction of air that has descended from higher altitudes or been transported from higher latitudes, where air has been more photochemically processed. The exact correlations between potential temperature and ClO and $ClONO_2$ are not universal in the atmosphere, e.g., the vertical gradient at midlatitudes as shown in Figs. 2a and 2b is gradual relative to the sharper increase that would be observed inside the wintertime polar vortex.

Figures 2c and 2d show ClO and $ClONO_2$ mixing ratios, respectively, now plotted with O_3 as the vertical coordinate. The blue, gray, and red points represent the same mixing ratios as in the upper panels, while the larger black points represent averages of ClO and $ClONO_2$ mixing ratios in 300 ppb O_3 bins. Relatively compact correlations between ozone as a vertical coordinate and daytime ClO and $ClONO_2$ mixing ratios are observed. This relation occurs because inorganic chlorine and ozone both have a strong positive correlation with age of air (outside the polar vortex). The formation of both inorganic chlorine and ozone involves processes that require photolysis of precursor molecules by solar UV radiation, with air at progressively higher altitudes and more polar latitudes on average having experienced greater cumulative UV exposure.

The peak mixing ratios observed during the DCOTSS mission were just under 30 ppt for ClO and just over 400 ppt for $ClONO_2$. Peak values for both species were observed in May 2022 and were unrelated to convection. The high values of $ClONO_2$ that lie to the right of the primary envelope of points in Fig. 2b (at $\theta \approx 410 – 430$ K and 440 – 490 K) are similarly from three flights in May 2022 and were also unrelated to convection. These points only appear as outliers when plotted versus potential temperature; they are unremarkable when plotted against O_3 in Fig. 2d, suggesting that large-scale dynamics is responsible. The variability in the observed mixing ratios of ClO and $ClONO_2$ for a given O_3 value in Fig. 2 is due to a combination of natural atmospheric variability and HAL instrument precision. The correlations are very tight, considering that the sampling took place over two different years and four different calendar months, over which inorganic chlorine is expected to vary. Despite extraordinary changes in the composition of the stratosphere in 2022 due to the Hunga volcanic eruption, no substantial perturbations were observed during the DCOTSS mission because the impacts of the Hunga eruption at that time occurred primarily at higher altitudes and farther south (Wilmouth et al., 2023; Santee et al., 2023; Østerstrøm et al., 2025).

3.2 Satellite Comparison

One useful way to examine the in situ measurements of ClO and $ClONO_2$ from the DCOTSS mission is to compare the aircraft data with existing satellite measurements. Figure 3 shows histograms of ClO data at 68 hPa for summers 2021 and 2022 from the ACE satellite instrument (Fig. 3a), the MLS satellite instrument (Fig. 3b), and the HAL instrument onboard the ER-2 during DCOTSS (Fig. 3c). The ACE and MLS satellite data represent all reported measurements after implementing the recommended filtering for June–August 2021 and 2022 over latitudes and longitudes approximately representing the contiguous United States. The 68 hPa level was chosen for comparison because this is a pressure level at which MLS data are reported (with vertical resolution of ~3 km), and 68 hPa is globally within the stratosphere, corresponding to approximately 19 km or 460 K during DCOTSS sampling. The

https://doi.org/10.5194/egusphere-2026-3480
Preprint. Discussion started: 25 June 2026

majority of the ACE measurements near 68 hPa are reported at 62 hPa or 73 hPa; for the purposes of this analysis, we include in Fig. 3 all reported ACE data in the 61–75 hPa pressure range. For the DCOTSS data from HAL, all in situ ClO data obtained in the 58–78 hPa pressure range are shown. The exact pressure range included is not critical to the overall comparison in Fig. 3.

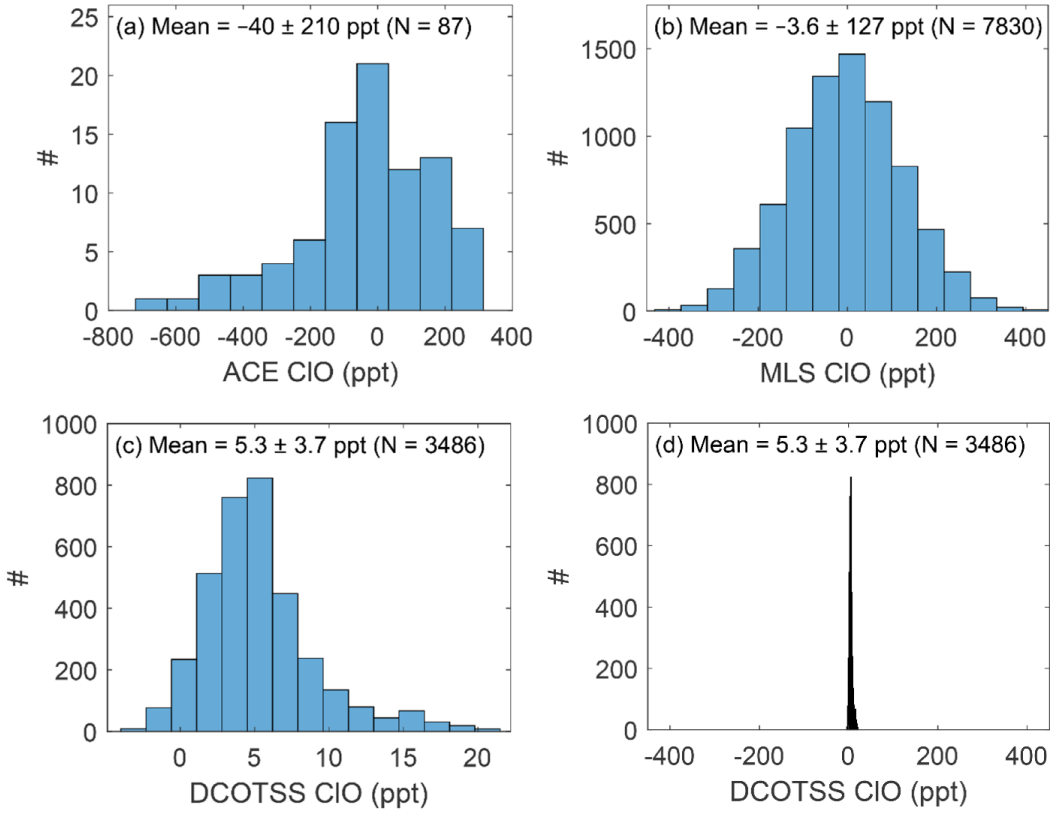

Figure 3. ClO measurements at the approximate 68 hPa pressure level during the summers of 2021 and 2022 over the contiguous U.S. (approximated as 30 – 50˚ N latitude, 70 – 125˚ W longitude) from satellite instruments and from the ER-2 during DCOTSS. The ClO data shown are from (a) the ACE satellite instrument using data in the 68 ± 7 hPa range for JJA in 2021 and 2022, (b) the MLS satellite instrument using reported data at 68 hPa for JJA in 2021 and 2022 and employing the recommended bias correction, and (c) the HAL instrument using all in situ data obtained at 68 ± 10 hPa from the 29 research flights of the DCOTSS mission 2021–2022. Panel (d) shows the same DCOTSS ClO data as in (c) but with the x-axis rescaled to match that of the MLS data in (b). At the top of each panel are listed the mean ClO value, the 1-sigma standard deviation, and the number of measurements (N) obtained over the 6 months of data collection.

Figure 3 shows that the range of ClO observations represented on the x-axes is dramatically narrower for the in situ data in panel 3c relative to the satellite data in panels 3a and 3b. The satellite data are at times hundreds of ppt negative or positive, while the total range from lowest to highest in situ observation is only about 25 ppt. ACE has very limited sampling over the northern midlatitudes in summertime, with only 87 data points over the 6 months total represented in Fig. 3a, while MLS has extensive coverage with 7830 total data points represented in Fig. 3b. Both

https://doi.org/10.5194/egusphere-2026-3480
Preprint. Discussion started: 25 June 2026

ACE and MLS ClO data for these 6 summer months have a negative mean and a very large standard deviation, as shown at the top of each figure panel. The in situ ClO data obtained by HAL during the DCOTSS mission include 3486 total data points and have a mean value of 5.3 ppt with a standard deviation of 3.7 ppt. Much of the spread in the in situ data is due to real atmospheric variability at 68±10 hPa rather than instrumental uncertainty. To better visualize the precision of the in situ data relative to the satellite data, Fig. 3d replots the same DCOTSS ClO data shown in Fig. 3c with the x-axis rescaled to match the x-axis of the MLS data in Fig. 3b. The precision of the in situ ClO data is more than an order of magnitude higher than that of the satellite data. Similar results are seen when comparing the ClO satellite data from ACE or MLS with the in situ ClO data from DCOTSS at higher and lower pressure levels relevant to ER-2 sampling (~50 – 150 hPa).

The intent of this satellite data analysis is to highlight that the in situ data obtained in DCOTSS are unique and that the excellent data quality allows stratospheric analyses that would otherwise not be possible. The limitations of the ClO satellite measurements are well known by the MLS and ACE data teams, and the results in Fig. 3 reflect the known accuracy and individual-profile precision of the data (Livesey et al., 2022; Boone et al., 2023). However, it is important to note that the satellite data at higher altitudes and deeper in the stratosphere, particularly those altitudes beyond the range of the ER-2, are significantly improved relative to the lower stratospheric ClO satellite data discussed here. Moreover, the higher mixing ratios of $ClONO_2$ relative to ClO allow the ACE measurements of $ClONO_2$ to become usable at a lower altitude than the ACE measurements of ClO. Supplement Fig. S3 shows a vertical profile comparison of $ClONO_2$ data from HAL during DCOTSS with all of the ACE satellite measurements of $ClONO_2$ for similar conditions as in Fig. 3. The preponderance of $ClONO_2$ data points from ACE are negative (below the detection limit) for pressures greater than ~80 hPa, but at lower pressures (higher altitudes, ~18 km and above), the ACE and DCOTSS data show good agreement. In the subsequent sections, we take advantage of the excellent precision and accuracy of the HAL data, using the in situ inorganic chlorine data from DCOTSS as the centerpiece of several analyses to examine our understanding of lower stratospheric chlorine chemistry.

3.3 Convection

One of the questions the DCOTSS mission sought to answer is whether perturbed inorganic chlorine mixing ratios would be observed in the stratosphere in the presence of elevated stratospheric water vapor following tropopause-overshooting convection in the NAMA. Non-catalytic reservoir species (HCl and $ClONO_2$) typically comprise more than 95% of total inorganic chlorine in the midlatitude lower stratosphere. However, enhanced water vapor in combination with cold temperatures in the NAMA can potentially enable repartitioning of Cl_y via heterogeneous reactions on ubiquitous binary sulfate-water aerosols (Anderson et al., 2012; Anderson et al., 2017; Robrecht et al., 2019). Under these conditions, HCl mixing ratios would be expected to decrease, while $ClONO_2$ mixing ratios would initially increase before later falling (Anderson et al., 2012). If elevated water vapor and low temperatures persisted long enough such that NO_x ($NO + NO_2$) was removed, elevated ClO would result, which in turn would lead to enhanced O_3 loss rates (Anderson et al., 2017). Two prior instances where ClO was measured in the lowermost stratosphere under conditions of elevated water vapor and aerosol surface area both showed substantially elevated ClO (Keim et al., 1996; Thornton et al., 2007).

https://doi.org/10.5194/egusphere-2026-3480
Preprint. Discussion started: 25 June 2026

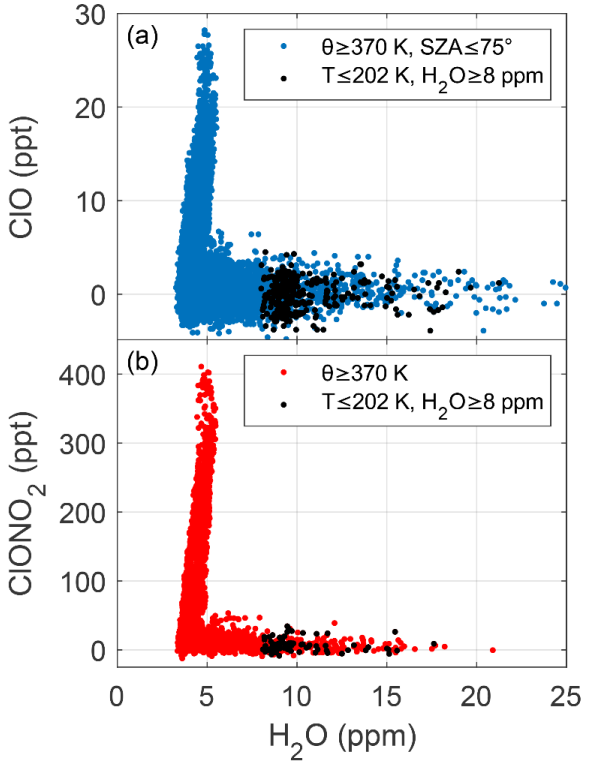

Figure 4. Stratospheric measurements of ClO and $ClONO_2$ relative to measured water vapor for all 29 research flights of the NASA DCOTSS mission. (a) ClO data are shown in blue for potential temperature ≥ 370 K and solar zenith angle ≤ 75˚, and (b) $ClONO_2$ data are shown in red for potential temperature ≥ 370 K. The black points in (a) and (b) represent the subset of data in each panel where observed temperature was ≤ 202 K and observed H_2O was ≥ 8 ppm.

Elevated water vapor in the stratosphere due to convective injection was targeted and frequently sampled during the DCOTSS mission (Homeyer et al., 2023; Homeyer et al., 2024; Bowman et al., 2026). Indeed, significantly more sampling of convectively influenced stratospheric air was achieved in this field campaign than in all previous in situ field campaigns combined (~28 hours; Homeyer et al., 2023). The relationship between water vapor up to 25 ppm and inorganic chlorine species as sampled over the entire DCOTSS mission is shown in Fig. 4. The data are filtered to focus on stratospheric measurements ($\theta \geq 370$ K), and the ClO data are additionally filtered to only include daytime values (SZA ≤ 75º). Both ClO (Fig. 4a) and $ClONO_2$ (Fig. 4b) are observed to have a similar L-shaped relationship with H_2O, for which the vertical portion represents the background stratosphere, with H_2O mixing ratios of typically 4–5 ppm, and the horizontal portion represents stratospheric air influenced by convection, with elevated H_2O. There were 23 additional measurements of ClO when H_2O was between 25 and 50 ppm (not shown for figure clarity), but these similarly lie near zero ClO and were acquired at temperatures exceeding 205 K.

https://doi.org/10.5194/egusphere-2026-3480
Preprint. Discussion started: 25 June 2026

The stratospheric conditions required to produce a significant change in inorganic chlorine partitioning following convection are a function of the water vapor mixing ratio and temperature, as well as the pressure and aerosol surface area (Anderson et al., 2012). In Fig. 4, we show black points overlaid in both panels indicating the subset of data where $H_2O \geq 8$ ppm and $T \leq 202$ K. The black points represent 2.2% of the overall data collected during the DCOTSS mission. As is evident in both panels, there were no observed instances in DCOTSS where either ClO or $ClONO_2$ was elevated in the presence of low temperatures and elevated water vapor. Even when H_2O was at the highest observed levels, thereby providing some relaxation to the low temperature constraint, perturbations to ClO and $ClONO_2$ were not observed. Multiple factors contributed to the lack of observed perturbations to inorganic chlorine partitioning in DCOTSS, but most importantly, most of the air that was sufficiently cold and wet during the mission tended to be very low in the stratosphere where inorganic chlorine mixing ratios are small. Also, the vast majority of DCOTSS sampling was of recent convection, so less time had elapsed for heterogeneous reactions to take place prior to observation. Further explanation for the absence of observed chlorine activation is provided in an extensive modeling study of DCOTSS data (Howar et al., 2025).

3.4 $ClONO_2$ Photochemistry and Kinetics

Chlorine nitrate is particularly important in stratospheric chemistry, as it is one of the two relatively long-lived reservoir species for inorganic chlorine (HCl being the other) and because it links the chlorine- and nitrogen-containing radical families (Stimpfle et al., 1999). The formation of $ClONO_2$ proceeds via a termolecular reaction of ClO with NO_2,

$$ClO + NO_2 + M \rightarrow ClONO_2 + M \quad \text{(R1)}$$

This reaction is also responsible for $ClONO_2$ being the primary reservoir for ClO at night outside of winter polar regions.

During the daytime, the primary loss mechanism for $ClONO_2$ is photolysis. Both $Cl + NO_3$ and $ClO + NO_2$ products are possible (Burkholder et al., 2019), but Cl and NO_3 products are rapidly converted to ClO and NO_2 in the stratosphere via reaction with O_3 and photolysis, respectively, so the net reaction of $ClONO_2$ photolysis for both product channels is

$$ClONO_2 + h\nu \rightarrow ClO + NO_2 \quad \text{(R2)}$$

With Reactions (R1) and (R2) dominating the formation and loss of $ClONO_2$ in the stratosphere, the concentration of $ClONO_2$ can be calculated using the photochemical steady-state approximation (Kawa et al., 1992; Stimpfle et al., 1999) as shown in Eq. (1).

$$[ClONO_2]_{ss} = \frac{k_{ClO+NO2}[ClO][NO_2]}{J_{ClONO2}} \quad (1)$$

Here square brackets denote concentration in molecule cm^{-3}, k is the second order rate coefficient for $ClONO_2$ production (R1) in cm^3 $molecule^{-1}$ s^{-1} and J is the photolysis rate coefficient (R2) in s^{-1}.

https://doi.org/10.5194/egusphere-2026-3480
Preprint. Discussion started: 25 June 2026

Figure 5a provides a demonstration of the interconnectedness between the mixing ratios of ClO and the photolysis of $ClONO_2$ in the stratosphere. Shown are the HAL ClO data from all DCOTSS research flights that included observations at solar zenith angle ≥ 60º at some point during the flight. The data are also filtered to include only higher altitudes (O_3 ≥ 1500 ppb) to restrict the analysis to similar air masses, although there is still scatter in the ClO data due to natural variability. Overall, mixing ratios of ClO clearly decrease with increasing solar zenith angle as expected, reaching 0 in darkness when SZA is approximately 92º. Overlaid on the ClO data is the photolysis rate of $ClONO_2$, which is in excellent qualitative agreement.

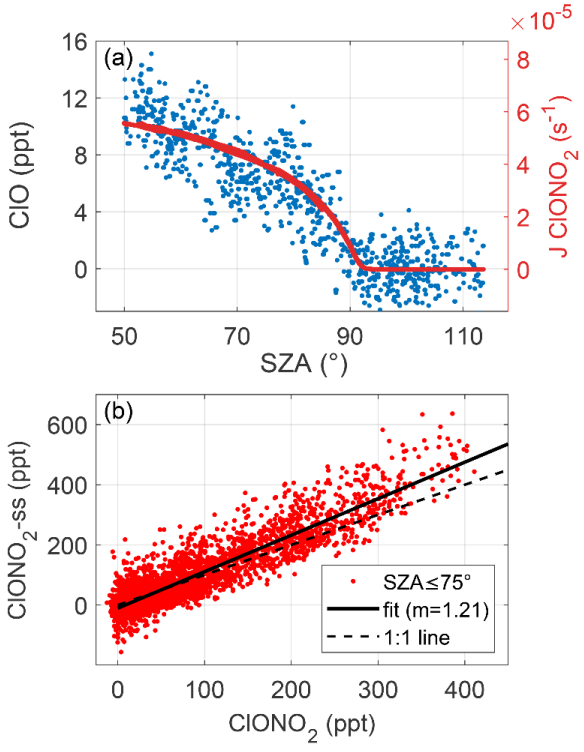

Figure 5. Inorganic chlorine photochemistry from measurements during the NASA DCOTSS mission. (a) Measured ClO as a function of solar zenith angle (blue) with the photolysis rate of $ClONO_2$ (red) overlaid. The data shown are from all the research flights that included observations at solar zenith angle ≥ 60˚ and were selected for higher altitudes with O_3 ≥ 1500 ppb. (b) Comparison of steady-state calculated $ClONO_2$ versus measured $ClONO_2$. The individual points (red) represent all available data from the 29 research flights of the DCOTSS mission filtered for solar zenith angle ≤ 75˚. The black solid line is a fit to the data, with slope of 1.21, and the black dashed line is the 1:1 line for reference. The number of data points plotted in (b) is 3602, which is less than the total number of $ClONO_2$ measurements at SZA ≤ 75º due to the requirement for simultaneous measurements of ClO, NO_2, O_3, and T.

To quantitively examine the ClO–$ClONO_2$ relationship, Fig. 5b shows steady-state $ClONO_2$ calculated as in Eq. (1) versus measured $ClONO_2$ from HAL for all 29 research flights of the DCOTSS mission. Measurements of ClO and NO_2 from the HAL and CANOE instruments on the ER-2 are used in the steady-state calculation, along with the

https://doi.org/10.5194/egusphere-2026-3480
Preprint. Discussion started: 25 June 2026

recommended values of $k_{ClO+NO2}$ from the latest NASA JPL compendium (Burkholder et al., 2019) and values of J_{ClONO2}, calculated as described in Section 2.2. The only filtering of the measured data is for SZA ≤ 75º to remove nighttime ClO. Overlaid on the data are a linear fit and the 1:1 line.

There is an excellent correlation between steady-state $ClONO_2$ and measured $ClONO_2$ mixing ratios during the DCOTSS mission. The relationship as shown in Fig. 5b is relatively compact and effectively linear. The slope of the fit line is 1.21 with y-intercept of –10. For $ClONO_2$ mixing ratios 25 ppt and greater, the maximum difference between the fit line and the 1:1 line is 19%, peaking at the highest measured mixing ratio of 411 ppt; the percent difference is 16% at 200 ppt and 11% at 100 ppt. The primary limitation on the accuracy of determining $ClONO_2$ from Eq. (1) is not the steady-state approximation itself, rather the uncertainties associated with the four variables that go into the equation. As discussed in Sections 2.1 and 2.2, the reported uncertainties of the ClO and NO_2 measurements are 17% and 10%, respectively, and the uncertainty in J_{ClONO2} is 10%. The largest uncertainty is in the JPL-recommended value of the production rate coefficient of $ClONO_2$, $k_{ClO+NO2}$, which is approximately 40% at the stratospheric temperatures considered here (Burkholder et al., 2019). Accounting for the uncertainties in the four variables on the righthand side of Eq. (1), the overall uncertainty in the steady-state calculated $ClONO_2$ mixing ratios is approximately 45%. By comparison, the uncertainty in measured $ClONO_2$ is 20%.

Given these uncertainties applicable to the x-axis (20%) and y-axis (45%) of Fig. 5b, the 19% or better level of agreement between steady-state calculated and measured $ClONO_2$ at all mixing ratios >25 ppt represents very good agreement within the total uncertainty. While the discrepancy between steady-state calculated and measured $ClONO_2$ is not statistically significant, we note that the direction of change needed for improvement is by increasing measured $ClONO_2$ or J_{ClONO2} or by decreasing measured ClO, measured NO_2, or $k_{ClO+NO2}$. The only individual value in the steady-state calculation of $ClONO_2$ (Eq. 1) with an uncertainty larger than 19% is $k_{ClO+NO2}$, suggesting that the JPL-recommended value may have a small high bias. Nevertheless, what can be stated with relatively high confidence, given the overall very good agreement shown in Fig. 5b, is that the large uncertainty in the JPL-recommended $ClONO_2$ production rate coefficient can be reduced.

3.5 Inorganic Chlorine Partitioning and Budget

HCl is a long-lived reservoir and the dominant form of inorganic chlorine in the stratosphere. Mixing ratios of HCl and O_3 have been observed to correlate linearly in the lower stratosphere, since both are produced primarily in the stratosphere and have long photochemical lifetimes, such that variations in their distributions are dominated by dynamical processes (Plumb and Ko, 1992; Marcy et al., 2004). Although HCl was not measured in situ during DCOTSS, we are able to calculate its mixing ratio for all flights of the mission using a technique that takes advantage of consistent relationships between HCl and O_3 in the lower stratosphere at altitudes accessible by the ER-2. MLS satellite data were utilized for this purpose. One difference here from past studies that focused on a fixed linear HCl:O_3 relationship in the upper troposphere and lowermost stratosphere (Marcy et al., 2004; Thornton et al., 2005; Marcy et al., 2007; Froidevaux et al., 2008; von Hobe et al., 2011; Jurkat et al., 2014; Wilkerson et al., 2021) is that we extend this analysis deeper into the stratosphere. More specifically, most previous studies did not exceed approximately 1000 ppb O_3 in a linear HCl:O_3 correlation plot, with 1450 ppb O_3 from a single balloon flight (Wilkerson et al., 2021)

https://doi.org/10.5194/egusphere-2026-3480
Preprint. Discussion started: 25 June 2026

representing the previous maximum to our knowledge, whereas for this study we examine values up to approximately 3000 ppb O_3. To do this, we determine HCl:O_3 ratios at the available MLS pressure levels but do not require that those ratios be the same at all pressure levels, as is implicit in previous studies at lower altitudes over a smaller vertical range. Using the HCl:O_3 ratios determined from each MLS retrieval pressure level as reference values, HCl mixing ratios during DCOTSS were calculated for each second of every flight using DCOTSS pressure and O_3 measurements. This approach works well, as demonstrated below.

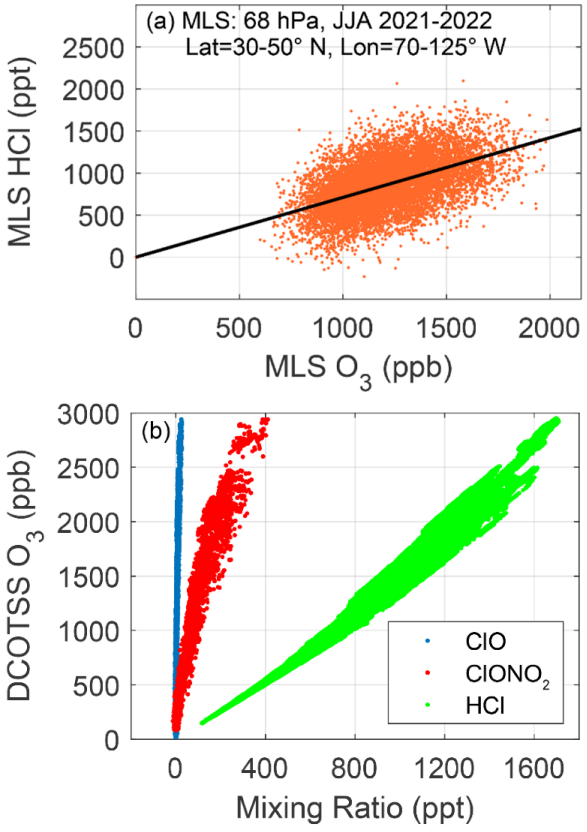

Figure 6. Measured HCl from MLS and calculated HCl for DCOTSS. (a) Scatter plot of HCl and O_3 measurements from the MLS satellite instrument obtained at 68 hPa during the summers of 2021 and 2022 over the approximate contiguous U.S. (30 – 50˚ N latitude, 70 – 125˚ W longitude). The slope of the fit line as shown is 0.71, or 7.1×10^{-4} when computed with HCl and O_3 in the same mixing ratio units (see text). The total number of points plotted is 10,100. (b) Inorganic chlorine data for all flights of the DCOTSS mission with DCOTSS O_3 as the vertical coordinate. HCl (green) is calculated as described in the text by determining the mean HCl:O_3 ratios from MLS at 100, 68 (shown in panel a), and 46 hPa and combining the interpolated slopes with high-resolution O_3 measurements from DCOTSS to produce HCl data for all DCOTSS flights. All ClO measurements (blue) for solar zenith angles ≤ 75˚ and $ClONO_2$ measurements (red) from DCOTSS are shown for reference. Calculated HCl is shown only for the P range 46 – 100 hPa. The number of HCl points shown is 355,876.

https://doi.org/10.5194/egusphere-2026-3480
Preprint. Discussion started: 25 June 2026

Figure 6a shows all concurrent measurements of HCl and O_3 acquired from MLS at the 68 hPa pressure level over the contiguous US in summers 2021 and 2022. Mean HCl at 68 hPa is 860 ppt and mean O_3 is 1210 ppb, yielding an HCl:O_3 ratio of 7.1×10^{-4} when in the same units. This value is the same as the slope acquired by fitting a line to the data plotted in Fig. 6a and forcing the small intercept of the fit line (39 ppt) to zero. Mean HCl:O_3 ratios and the corresponding scatter plots with fit lines of HCl and O_3 were similarly generated for the other relevant MLS pressure levels, resulting in mean HCl:O_3 ratios of 8.0×10^{-4} at 100 hPa and 5.6×10^{-4} at 46 hPa. The estimated uncertainties in the mean ratios, based on the reported pressure-dependent accuracies of the MLS HCl and O_3 data (Livesey et al., 2022), are 0.9×10^{-4}, 1.6×10^{-4}, and 0.6×10^{-4} at 68, 100, and 46 hPa, respectively. The HCl:O_3 ratios for all pressure levels between 46 and 100 hPa were produced by interpolating between the three available MLS pressure levels. Supplement Fig. S4 shows scatter plots of HCl versus O_3 mixing ratios for the three MLS pressure levels discussed here as well as 32 hPa, where the HCl:O_3 relationship is substantially different. It is evident from this plot that O_3 mixing ratios rise faster than HCl mixing ratios deeper in the stratosphere, necessitating using a different HCl:O_3 ratio for the lower pressures of this study. The 46 – 100 hPa pressure range covers the vertical extent of nearly all stratospheric data obtained during the DCOTSS mission (see Fig. S2).

Using the MLS-derived conversion factors described above, in combination with in situ O_3 mixing ratios and pressure data from instrumentation on the ER-2, mixing ratios of HCl at high time resolution were calculated for all DCOTSS flights, as shown in Fig. 6b. DCOTSS in situ O_3 is the vertical coordinate, with HCl data shown for the pressure range 46 – 100 hPa. Also shown for reference are ClO (filtered for daytime, SZA ≤ 75º) and $ClONO_2$ measured in situ from the HAL instrument, as previously plotted in Figs. 2c and 2d. The inorganic chlorine mixing ratios in Fig. 6b appear as expected, with the radical ClO having the smallest mixing ratios, followed by the reservoir species $ClONO_2$, followed by the longer-lived dominant reservoir HCl. Consistent with previously discussed increases in ClO and $ClONO_2$ that correlate with increases in potential temperature or O_3, HCl values increase dramatically with higher O_3 mixing ratios in Fig. 6b. The scatter in the data is low, with a relatively tight spread in the individual variables. There are a range of pressure levels represented by each O_3 mixing ratio, which is driving the spread in the calculated HCl data.

To quantitatively examine inorganic chlorine partitioning in the midlatitude lower stratosphere, we ratio measured ClO, measured $ClONO_2$, and calculated HCl to the sum of these three mixing ratios, $Cl_y^{sum} \approx ClO + ClONO_2 + HCl$. Fig. 7a shows this partitioning for all research flights of the DCOTSS mission as a function of potential temperature. Due to the more limited vertical range of calculated HCl data, the lower limit of the potential temperatures shown is approximately 390 K, which represents exclusively stratospheric air during DCOTSS. HCl is the dominant form of inorganic chlorine at all potential temperatures in Fig. 7a, especially at the lowest levels. Complementary to Fig. 6b, which shows universal increases in ClO, $ClONO_2$, and HCl mixing ratios as organic chlorine-containing compounds are converted to inorganic form deeper in the stratosphere, Fig. 7a shows that the fractional contribution of HCl to total inorganic chlorine decreases with θ in the stratosphere due to repartitioning. Over the 390 – 520 K potential temperature range, the fraction of total inorganic chlorine in the form of HCl decreases from approximately 0.96 (±0.03) to 0.84 (±0.03), while the fraction of $ClONO_2$ increases from approximately 0.04 (±0.02) to 0.15 (±0.02), and the fraction of ClO increases from approximately 0.001 (±0.006) to 0.01 (±0.002). Listed uncertainties represent the

https://doi.org/10.5194/egusphere-2026-3480
Preprint. Discussion started: 25 June 2026

calculated standard deviations. Despite the relatively small fractional contribution of ClO to total inorganic chlorine, ClO exerts significant control over stratospheric ozone due to the catalytic nature of ozone loss reactions.

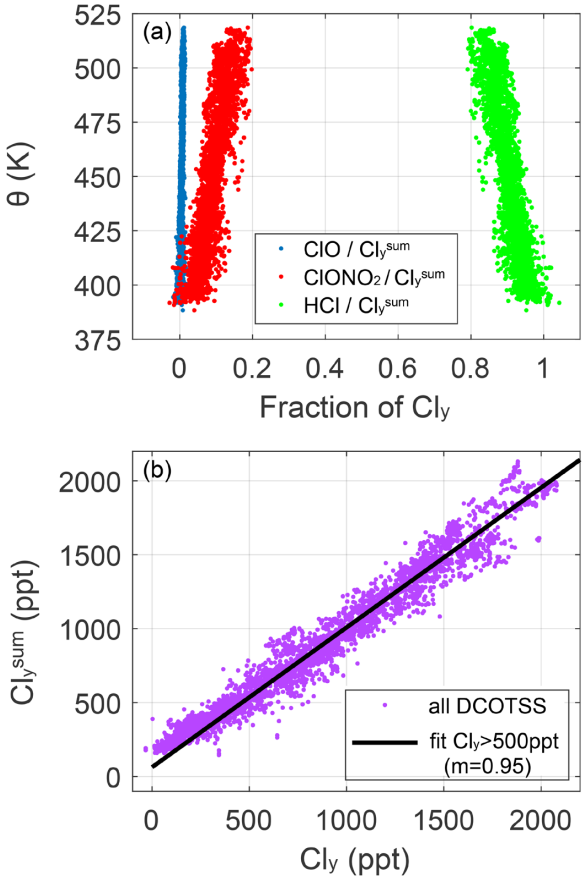

Figure 7. Inorganic chlorine partitioning and budget in the stratosphere during the NASA DCOTSS mission. (a) Ratios of measured ClO (blue), measured $ClONO_2$ (red), and calculated HCl (green) to the sum of the mixing ratios of these inorganic chlorine compounds, Cl_y^{sum}. The ClO measurements are only shown for solar zenith angle ≤ 75°. (b) Sum of all ClO, $ClONO_2$, and HCl data from DCOTSS versus total inorganic chlorine, Cl_y, independently calculated using measurements of organic chlorine compounds. The fit line (black) is for data with Cl_y > 500 ppt and has a slope of 0.95. The vertical range represented corresponds to 46 – 100 hPa, the pressures over which calculated HCl mixing ratios are available. The total number of points plotted in (b) is 3666, a number set by the requirement for concurrent availability of all measurements.

An important test of the accuracy of the inorganic chlorine mixing ratios determined in this study, and a critical evaluation of our understanding of midlatitude chlorine chemistry more generally, is to evaluate the chlorine budget during the DCOTSS mission. Specifically, we compare agreement between the sum of the individual mixing ratios (Cl_y^{sum}, as defined above) and total inorganic chlorine (Cl_y), which is independently calculated from organic chlorine

https://doi.org/10.5194/egusphere-2026-3480
Preprint. Discussion started: 25 June 2026

compounds measured on the ER-2, as described in Section 2.2. Fig. 7b shows this comparison, using all data from the 29 DCOTSS research flights, filtered to include only daytime ClO (SZA ≤ 75º). The agreement in Fig. 7b between Cl_y^{sum} and calculated Cl_y is highly robust. The relationship is linear, and a fit of all data points where Cl_y is greater than 500 ppt produces a slope of 0.95. The uncertainty in calculated Cl_y is relatively small, so this level of agreement is a testament to the accuracy of the ClO and $ClONO_2$ in situ measurements as well as the approach used here for calculating HCl. Moreover, this result supports the accuracy of measured $ClONO_2$ and ClO as it pertains to the differences discussed in Section 3.4 between measured and steady-state calculated $ClONO_2$. To our knowledge, the agreement of Cl_y^{sum} and Cl_y to within 5% represents the best inorganic chlorine budget agreement ever obtained using in situ ER-2 data, including missions where the budget was deemed to be in agreement, such as POLARIS at northern high latitudes in summertime (Bonne et al., 2000) and SOLVE-THESEO in the Arctic vortex when inorganic chlorine was nearly fully activated in wintertime (Wilmouth et al., 2006).

Despite the overall excellent budget agreement for the DCOTSS mission, the data below approximately 500 ppt in Fig. 7b deviate from the fit line, and even more so from the 1:1 line. Specifically, Cl_y^{sum} becomes increasingly high relative to total inorganic chlorine as Cl_y decreases below 500 ppt, with the value of Cl_y^{sum} approximately 170 ppt at 0 ppt Cl_y. We consider three possibilities to explain this discrepancy: (1) Measured ClO or measured $ClONO_2$ is too high. This cannot be the cause, as ClO and $ClONO_2$ mixing ratios are not large enough at these Cl_y levels to resolve the issue even if reduced to zero. (2) Our calculated HCl is biased high at low mixing ratios. This would likely require a high bias in the MLS measurement of HCl or a low bias in the MLS measurement of O_3 in the lowermost stratosphere. The HCl:O_3 slope found here at 100 hPa (8.0×10^{-4}) agrees very well with the value (~8×10^{-4}) of Jurkat et al. (2014) but is higher than values (~5×10^{-4}) from two earlier aircraft studies (Marcy et al., 2004; von Hobe et al., 2011); however, given the measurement uncertainties and expected differences between the studies due to different latitudes being sampled, the results are consistent. We note that it is very unlikely that DCOTSS O_3 used to calculate HCl is biased high at low mixing ratios, because O_3 was measured by two independent instruments (ROZE and UCATS) and the two data sets agree. (3) Finally, we consider that Cl_y determined from organics might be biased low at low mixing ratios. If true, this could resolve the discrepancy in Fig. 7b below 500 ppt by shifting Cl_y to the right rather than shifting Cl_y^{sum} down. The small estimated uncertainty of 6% for Cl_y > 500 ppt increases substantially as mixing ratios decrease, exceeding a factor of 2 at the smallest mixing ratios, due largely to the difficulties in accurately defining the total organic chlorine content at the tropopause of the sampled stratospheric airmasses, as well as the precise contribution to Cl_y from the decomposition of VSL species (Howar et al., 2025). Ultimately, the overall agreement in Fig. 7b is excellent, and while the disagreement between Cl_y^{sum} and Cl_y at the lowest values appears systematic, it is small and generally within the estimated uncertainties.

3.6 Wildfire Aerosol

The Australian New Year's (ANY) fires of December 2019 and January 2020 were responsible for injecting a record quantity of biomass burning products into the Southern Hemisphere midlatitude stratosphere and led to unexpected, dramatic perturbations to stratospheric composition in the months following the fires due to changes in dynamics and chemistry (Khaykin et al., 2020; Santee et al., 2022; Strahan et al., 2022; Salawitch and McBride, 2022;

https://doi.org/10.5194/egusphere-2026-3480
Preprint. Discussion started: 25 June 2026

Solomon et al., 2023; Ma et al., 2024). In particular, there were substantial changes to the stratospheric chlorine species, namely suppression of HCl and concomitant increases in ClO and $ClONO_2$, as measured by the MLS and ACE satellite instruments. These observed changes could not be reproduced in models using typical chlorine heterogeneous reactions known to be important at cold temperatures (e.g., HCl + $ClONO_2$) or using the N_2O_5 hydrolysis reaction known to be enhanced following volcanic eruptions (Strahan et al., 2022, Solomon et al., 2023).

Solomon et al. (2023) proposed a new mechanism to explain the perturbed stratospheric inorganic chlorine chemistry following the ANY fires, which was able to reasonably reproduce the MLS and ACE satellite observations of ClO, $ClONO_2$, and HCl. In this mechanism, HCl solubility is posited to be greatly increased due to the presence of a high fraction of organic species in aged biomass burning aerosol, allowing heterogeneous chlorine activation at far warmer temperatures than previously considered possible. Stone et al. (2025) subsequently modeled the stratospheric impact of the ANY fires for the 2 years after their occurrence, highlighting better results when HCl solubility in wildfire organic aerosols is modeled differently from stratospheric background organic aerosols. In theory, if the Solomon et al. (2023) mechanism is correct, the presence of biomass burning organic aerosol could allow for HCl uptake and initiate heterogeneous chemical reactions that reduce HCl and enhance $ClONO_2$ and ClO at temperatures typical of the midlatitude lower stratosphere during DCOTSS.

Instrumentation on board the ER-2 during the DCOTSS mission provided several measurements that enable us to test the relationship between organic aerosol and inorganic chlorine in the midlatitude stratosphere. In particular, aerosol composition measurements from the PALMS-NG instrument were used to generate organic mass fraction (OMF) and biomass burning fraction (BBF) data products. OMF is defined as the ratio of organic mass to the combined mass of organics and sulfate, i.e., Org / (Org + Sulf). This quantity is derived from laboratory calibrations and calculated only for non-refractory particle types, including internally mixed sulfate–organic particles, biomass burning, and meteoric particles. BBF is defined as the number fraction of particles characterized by strong mass spectral signals of potassium and organic species and attributed directly to a biomass burning origin. During past flights, the PALMS instrument acquired mass spectra within biomass burning plumes; particles contained carbon, potassium, organics, and ammonium ions but not pure soot. These mass spectra were used to develop a biomass-burning particle signature for subsequent characterization (Hudson et al., 2004). Particle identification and organic mass calibration follow methods previously described (Froyd et al., 2019) and have been refined for DCOTSS flights (Shen et al., 2025).

Figure 8 shows scatter plots of ClO and $ClONO_2$ mixing ratios measured by HAL versus OMF and BBF reported by PALMS-NG. Data are shown for all 16 flights where the aerosol data are available, i.e., the DCOTSS flights in 2022, and are exclusively in the stratosphere ($\theta > 390$ K). The black line in each panel represents a least-squares fit to the data. The four panels of Fig. 8 show that ClO and $ClONO_2$ mixing ratios decrease with increasing organic mass fraction and biomass burning fraction. This result is inconsistent with what might have been expected if the Solomon et al. (2023) mechanism had been significant in the Northern Hemisphere midlatitudes during the sampling period of the DCOTSS mission. It is important to note that the negative correlations in the panels of Fig. 8 are not causal; ClO and $ClONO_2$ reliably increased as a function of potential temperature (age of air) during DCOTSS, while OMF and BBF both typically decreased with θ (more significantly for OMF), which results in negative correlations when these

https://doi.org/10.5194/egusphere-2026-3480
Preprint. Discussion started: 25 June 2026

variables are plotted against one another. That said, if significant HCl uptake on organic aerosol and heterogeneous chlorine activation had occurred in DCOTSS 2022 due to high OMF and/or BBF, we would have expected to see anomalously high ClO or $ClONO_2$ mixing ratios toward the righthand sides of the panels in Fig. 8. The data are noisy, but there are no obvious ClO or $ClONO_2$ enhancements. Supplement Fig. S5 shows similar results in analogous plots to Fig. 8, with ClO and $ClONO_2$ plotted as a fraction of Cl_y. The earlier analyses in this paper (e.g., Fig. 2) confirm that ClO and $ClONO_2$ were not significantly perturbed during the mission.

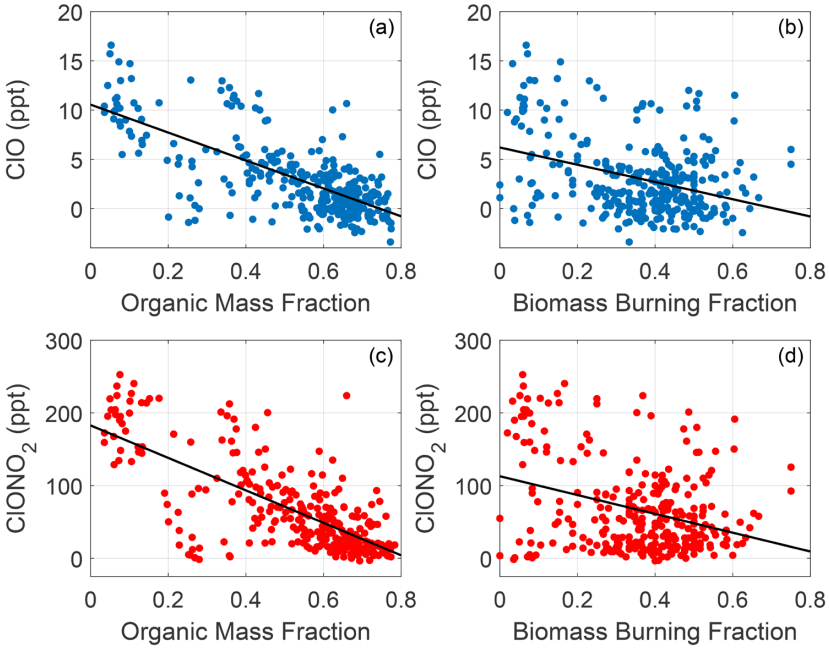

Figure 8. Scatter plots of ClO mixing ratios from HAL with (a) organic mass fraction and (b) biomass burning fraction (by particle number) from PALMS-NG; (c) and (d) analogous plots for $ClONO_2$. Plotted are data from the 16 DCOTSS flights (all in 2022) where aerosol fractional values were reported; data shown are for potential temperature ≥ 390 K, and ClO measurements are only shown for solar zenith angle ≤ 75˚. Due to the relatively sparse reporting of the aerosol fractional data, the inorganic chlorine data are interpolated to the fractional data; this introduces very little error. The black lines in each panel represent least-squares fits to the data.

This null result should not be extended to comment on the specific conditions of the ANY fires. However, the result does appear to show that the Solomon et al. (2023) mechanism was not pervasive in the background midlatitude lower stratosphere during DCOTSS, even though organic species in biomass burning aerosol were present and temperatures were sufficiently cold. The presence of biomass burning organic aerosols in the DCOTSS-sampled air masses is supported by independent measurements from multiple instruments (Sharpe et al., 2026). One relevant consideration with respect to chlorine activation is that the DCOTSS sampling was in summertime, and Stone et al. (2025) found a significant seasonal impact of the ANY fires due to photochemistry, with perturbations to inorganic chlorine in wintertime being dominant relative to other seasons. Also, as noted by Chipperfield and Bekki (2024) and

https://doi.org/10.5194/egusphere-2026-3480
Preprint. Discussion started: 25 June 2026

Stone et al. (2025), the physical state (liquid, glassy, solid) and detailed composition of the aerosol are important factors and were not known for the ANY fires, which prevents us from comparing with DCOTSS. Further study, particularly in the laboratory, is needed to better predict the impact of wildfires and organic aerosol on stratospheric chlorine and the ozone layer.

4 Conclusions

In situ inorganic chlorine measurements of ClO and $ClONO_2$ were obtained from the ER-2 aircraft over a total of 6 months in the summers of 2021 and 2022 as part of the NASA DCOTSS mission over Northern Hemisphere midlatitudes. The precision of the chlorine data from the HAL instrument was excellent throughout the campaign, to our knowledge the best ever obtained from an aircraft platform at these altitudes: 2 ppt for ClO and 5 ppt for $ClONO_2$ in 35 sec and, with averaging, a detection limit of under 1 ppt for ClO and 2 ppt for $ClONO_2$. In particular, the ClO data from HAL have more than an order of magnitude higher precision than MLS and ACE satellite data for many of the lower stratospheric altitudes studied here, enabling analyses that would not otherwise be possible.

Analysis of the in situ ClO and $ClONO_2$ measurements shows a relatively compact distribution and increasing mixing ratios with potential temperature or ozone as the vertical coordinate, consistent with all four variables increasing with age of air in the lower stratosphere. Other than ClO mixing ratios going to zero at night as expected, there were no substantial outliers in the vertical profiles of ClO or $ClONO_2$, especially when plotted against O_3. The lack of substantial outliers represents an important scientific result, as discussed below, and also speaks to the quality of the data set for performing tests of stratospheric inorganic chlorine chemistry. The peak ClO and $ClONO_2$ mixing ratios observed during the DCOTSS mission were approximately 30 ppt and 400 ppt, respectively.

One of the key questions of the DCOTSS campaign is whether chlorine activation would be observed in the lower stratosphere in the presence of low temperatures and elevated water vapor from convective injection, as suggested by several modeling studies. We found no significant difference in measured ClO or $ClONO_2$ mixing ratios during the mission regardless of whether the sampled air had enhanced water vapor and low temperatures. One factor contributing to this result is that most of the air sampled in DCOTSS that was sufficiently cold and wet to accelerate heterogeneous chlorine reactions was located very low in the stratosphere, with small inorganic chlorine mixing ratios. Also, most DCOTSS sampling of enhanced water vapor followed recent convection because it was more easily targeted in flight planning, but this meant that not much time had elapsed for the relatively slow heterogeneous chlorine reactions to take place prior to ER-2 intercept. While this null result from the two years of DCOTSS sampling suggests that chlorine activation is not pervasive in the Northern Hemisphere midlatitude summer stratosphere following overshooting convection, it cannot be interpreted to mean that inorganic chlorine is never perturbed there: (1) Despite the relatively extensive sampling during the DCOTSS mission, only a small fraction of all convective events in the summers of 2021 and 2022 were sampled; (2) there is significant interannual variability in stratospheric conditions, so sampling other summers could yield different results; and (3) the presence of elevated aerosol surface area beyond 2021–2022 levels in conjunction with enhanced water vapor mixing ratios and low temperatures would make the stratosphere much more vulnerable to chlorine activation following convection, as recently demonstrated by Howar et al. (2025).

https://doi.org/10.5194/egusphere-2026-3480
Preprint. Discussion started: 25 June 2026

The production and loss mechanisms used to calculate photochemical steady-state mixing ratios of $ClONO_2$ in the lower stratosphere were found to be in good agreement with in situ measurements of $ClONO_2$ throughout the DCOTSS mission. A scatter plot of steady-state versus measured $ClONO_2$ is relatively compact and linear across the full range of mixing ratios, with a slope of 1.21 and agreement to within 19% or better for $ClONO_2$ > 25 ppt. This level of agreement is much smaller than the uncertainty of the steady-state calculated values (45%), suggesting that the uncertainty in the JPL-recommended $ClONO_2$ production rate coefficient, $k_{ClO+NO2}$, which represents by far the largest uncertainty in the calculation, can be reduced.

HCl, the largest stratospheric reservoir of inorganic chlorine, was not measured on the ER-2 during the DCOTSS mission, but we calculate HCl mixing ratios in this study at high time resolution for every research flight. This was accomplished by establishing the HCl:O_3 relationship from MLS measurements at the available MLS retrieval pressure levels (100, 68, and 46 hPa) corresponding to ER-2 stratospheric altitudes, interpolating those ratios against pressure to fill in the measurement gaps, and then multiplying the interpolated values as a function of pressure by measured in situ O_3. The HCl calculated in this manner overall appears very well behaved and accurate. HCl dominates inorganic chlorine partitioning but decreases approximately 12% as potential temperature rises from 390 to 520 K, while $ClONO_2$ and ClO partitioning increase substantially.

Further evaluation of the inorganic chlorine chemistry observed in DCOTSS involves determination of the inorganic chlorine budget. We find that the sum of ClO + $ClONO_2$ + HCl (Cl_y^{sum}) is in excellent agreement with total inorganic chlorine (Cl_y), which is independently determined from measurements of organic chlorine compounds. For mixing ratios greater than 500 ppt, the agreement between Cl_y^{sum} and Cl_y is within 5% (slope of 0.95 when plotting Cl_y^{sum} vs Cl_y), representing the best inorganic chlorine budget agreement ever obtained on the ER-2 to our knowledge. There is a small disagreement between Cl_y^{sum} and Cl_y at mixing ratios below approximately 500 ppt that appears to become larger approaching the origin. Despite this disparity generally being within the uncertainty, it appears to be systematic. Some potential factors giving rise to this discrepancy can be ruled out entirely, with a high bias in calculated HCl or a low bias in Cl_y at the lowest mixing ratios being the most likely cause.

Finally, we consider the potential impact of aged organic aerosols on inorganic chlorine mixing ratios. Solomon et al. (2023) previously proposed a new mechanism to explain the large stratospheric reductions in HCl and increases in ClO and $ClONO_2$ following the ANY fires in 2019–2020 in which HCl solubility is greatly increased due to the presence of a high fraction of organic species in the biomass burning aerosol, which would allow heterogeneous chlorine activation to occur at temperatures commonly found throughout the midlatitude lower stratosphere. During the DCOTSS mission, we did not observe any evidence of this mechanism occurring in the Northern Hemisphere midlatitude stratosphere, even when organic mass fraction and biomass burning fraction were elevated. This null result should not be interpreted as a challenge to the Solomon et al. (2023) mechanism for explaining the changes to stratospheric inorganic chlorine observed following the ANY fires. Rather, the DCOTSS observations provide an important data point for how pervasive the mechanism may be in the global stratosphere in the presence of organic and biomass burning aerosols.

Looking ahead, the future of stratospheric chlorine measurements is uncertain (Salawitch et al., 2025). The MLS satellite instrument will soon be taken out of service, and while ACE is still producing data, it has relatively sparse

https://doi.org/10.5194/egusphere-2026-3480
Preprint. Discussion started: 25 June 2026

observational coverage outside of the high latitudes and is well beyond its expected lifetime. Opportunities for in situ measurement of stratospheric chemistry like the DCOTSS mission are infrequent. The future holds many unknowns for possible perturbations to inorganic chlorine and ozone in the stratosphere due to influences such as intense wildfires, volcanic eruptions, rocket launches and space metal reentry, VSL chlorine emissions, increasing water vapor, decreasing temperatures, and potential climate intervention strategies. The consistently well-behaved measurements of ClO and $ClONO_2$ during the DCOTSS mission, despite sampling in many different types of air masses, provide valuable insight into the current stratosphere and serve as a point of reference for future studies in light of potential stratospheric perturbations on the horizon.

Code and data availability

All data utilized in this study are publicly available. Data from the DCOTSS project can be obtained from the NASA Atmospheric Science Data Center at https://doi.org/10.5067/ASDC/DCOTSS-Aircraft-Data_1. Aura Microwave Limb Sounder (MLS) data are publicly available at https://search.earthdata.nasa.gov/search?fi=MLS. ACE-FTS data are available at https://databace.scisat.ca. Photodissociation frequencies computed along the DCOTSS flight tracks are available at https://doi.org/10.5281/zenodo.14968099.

Author contributions

DMW conceptualized the paper, performed the data analysis and visualization, and prepared the manuscript with contributions from all co-authors. All authors were involved in data collection essential to this study: DMW, JSH, and JGA for inorganic chlorine; LVH and RJS for total inorganic chlorine and photolysis rates; EJH for total inorganic chlorine and ozone; JBS, DSS, DMW, JSH, and JGA for water vapor; JMSC, ERD, RAH, and TFH for nitrogen dioxide and ozone; DJC and XS for aerosols; MLS for MLS satellite data; TPB for meteorology; CRH, PAN, and KPB for flight planning; KPB and FNK for DCOTSS mission leadership.

Competing interests

One of the co-authors is a member of the editorial board of Atmospheric Chemistry and Physics.

Acknowledgments

We are grateful to the ER-2 pilots and crew as well as the entire DCOTSS team for their efforts, which resulted in a successful project and enabled the measurements for this study. We thank the MLS and ACE-FTS teams for the satellite data used in this study.

Financial support

This work was supported by the National Aeronautics and Space Administration (NASA) under the Earth Venture Suborbital-3 program awards for DCOTSS (80NSSC19K0326, 80NSSC19K1399, 80NSSC19K1058, 80NSSC19K0347, 80NSSC19K0341). Work at the Jet Propulsion Laboratory, California Institute of Technology, was carried out under a contract with NASA (80NM0018D0004). Additional support was provided by the U.S. National

https://doi.org/10.5194/egusphere-2026-3480
Preprint. Discussion started: 25 June 2026

Science Foundation (NSF), Grant No. 2426145. DMW acknowledges support for this work while serving at NSF; any opinions, findings, conclusions, or recommendations expressed in this publication are those of the authors and do not necessarily reflect the views of NSF or the U.S. government.

References

Anderson, J. G, Margitan, J. J., and Stedman, D. H.: Atomic chlorine and the chlorine monoxide radical in the stratosphere: three in situ observations, Science, 198, 501–503, doi:10.1126/science.198.4316.501, 1977.

Anderson, J. G., Brune, W. H., and Toohey, D. W.: Free radicals within the Antarctic vortex: the role of CFCs in Antarctic ozone loss. Science, 251, 39–46, doi:10.1126/science.251.4989.39, 1991.

Anderson, J. G., Wilmouth, D. M., Smith, J. B., and Sayres, D. S.: UV dosage levels in summer: Increased risk of ozone loss from convectively injected water vapor, Science, 337, 835–839, doi:10.1126/science.1222978, 2012.

Anderson, J. G., Weisenstein, D. K., Bowman, K. P., Homeyer, C. R., Smith, J. B., Wilmouth, D. M., Sayres, D. S., Klobas, J. E., Leroy, S. S., Dykema, J. A., and Wofsy, S. C.: Stratospheric ozone over the United States in summer linked to observations of convection and temperature via chlorine and bromine catalysis, Proc. Natl. Acad. Sci. USA, 114, e4905–e4913, doi:10.1073/pnas.1619318114, 2017.

Ansmann, A., Ohneiser, K., Chudnovsky, A., Knopf, D. A., Eloranta, E. W., Villanueva, D., Seifert, P., Radenz, M., Barja, B., Zamorano, F., Jimenez, C., Engelmann, R., Baars, H., Griesche, H., Hofer, J., Althausen, D., and Wandinger, U.: Ozone depletion in the Arctic and Antarctic stratosphere induced by wildfire smoke, Atmos. Chem. Phys., 22, 11701–11726, https://doi.org/10.5194/acp-22-11701-2022, 2022.

Boone, C. D., Bernath, P. F., and Lecours, M.: Version 5 retrievals for ACE-FTS and ACE-imagers, J. Quant. Spectrosc. Radiat. Transf., 310, 108749, doi:10.1016/j.jqsrt.2023.108749, 2023.

Bowman, K. B., Keutsch, F. N., Homeyer, C. R., Sayres, D. S., Smith, J. B., Wilmouth, D. M., Anderson, J. G., Atlas, E. L., Apel, E., Bedka, K., Bui, T. P., Cziczo, D., Daube, B., Delaria, E. R., Dykema, J., Hanisco, T. F., Hannun, R., Hall, B., Hintsa, E., Howar, L., Hurst, D., Jacquot, J. L., Laskin, A., Li, Y., Liu, C., Moore, F., Mullendore, G., Newman, P., Pandit, A. K., Rapp, A. D., Salawitch, R. J., Shen, X., St. Clair, J. M., Ueyama, R., Vernier, J.-P., and Wofsy, S. C., The Dynamics and Chemistry of the Summer Stratosphere (DCOTSS) Project, Bull. Amer. Meteor. Soc., 107, E696–E717, doi:10.1175/BAMS-D-24-0177.1, 2026.

Burkholder, J. B., Sander, S. P., Abbatt, J., Barker, J. R., Cappa, C., Crounse, J. D., Dibble, T. S., Huie, R. E., Kolb, C. E., Kurylo, M. J., Orkin, V. L., Percival, C. J., Wilmouth, D. M., and Wine, P. H.: Chemical Kinetics and Photochemical Data for Use in Atmospheric Studies, Evaluation No. 19, JPL Publication 19-5, Jet Propulsion Laboratory, Pasadena, http://jpldataeval.jpl.nasa.gov, 2019.

Brune, W. H., Anderson, J. G., and Chan, K. R.: In situ observations of ClO in the Antarctic: ER-2 aircraft results from 54°S to 72°S latitude, J. Geophys. Res., 94, 16649–16663, doi:10.1029/JD094iD14p16649, 1989.

Chipperfield, M. P. and Bekki, S.: Opinion: Stratospheric ozone–depletion, recovery and new challenges, Atmos. Chem. Phys., 24, 2783–2802, doi:10.5194/acp-24-2783-2024, 2024.

Cooney, J. W., Bowman, K. P., Homeyer, C. R., and Fenske, T. M.: Ten-year analysis of tropopause-overshooting convection using GridRad data. J. Geophys. Res. Atmos., 123, 329–343, doi:10.1002/2017JD027718, 2018.

https://doi.org/10.5194/egusphere-2026-3480
Preprint. Discussion started: 25 June 2026

Ellis, T. M., Bowman, D. M. J. S., Jain, P., Flannigan, M. D., and Williamson, G. J.: Global increase in wildfire risk due to climate-driven declines in fuel moisture, Glob. Change Biol., 28, 1544–1559, doi:10.1111/gcb.16006, 2022.

Froidevaux, L., Jiang, Y. B., Lambert, A., Livesey, N. J., Read, W. G., Waters, J. W., Fuller, R. A., Marcy, T. P., Popp, P. J., Gao, R. S., Fahey, D. W., Jucks, K. W., Stachnik, R. A., Toon, G. C., Christensen, L. E., Webster, C. R., Bernath, P. F., Boone, C. D., Walker, K. A., Pumphrey, H. C., Harwood, R. S., Manney, G. L., Schwartz, M. J., Daffer, W. H., Drouin, B. J., Cofield, R. E., Cuddy, D. T., Jarnot, R. F., Knosp, B. W., Perun, V. S., Snyder, W. V., Stek, P. C., Thurstans, R. P., and Wagner, P. A.: Validation of Aura Microwave Limb Sounder HCl measurements, J. Geophys. Res., 113, D15S25, doi:10.1029/2007JD009025, 2008.

Froyd, K. D., Murphy, D. M., Brock, C. A., Campuzano-Jost, P., Dibb, J. E., Jimenez, J.-L., Kupc, A., Middlebrook, A. M., Schill, G. P., Thornhill, K. L., Williamson, C. J., Wilson, J. C., and Ziemba, L. D.: A new method to quantify mineral dust and other aerosol species from aircraft platforms using single-particle mass spectrometry, Atmos. Meas. Tech., 12, 6209–6239, doi:10.5194/amt-12-6209-2019, 2019.

Fromm, M., Servranckx, R., Stocks, B. J., and Peterson, D. A.: Understanding the critical elements of the pyrocumulonimbus storm sparked by high-intensity wildland fire, Commun. Earth Environ., 3, 243, doi:10.1038/s43247-022-00566-8, 2022.

Hannun, R. A., Swanson, A. K., Bailey, S. A., Hanisco, T. F., Bui, T. P., Bourgeois, I., Peischl, J., and Ryerson, T. B.: A cavity-enhanced ultraviolet absorption instrument for high-precision, fast-time-response ozone measurements, Atmos. Meas. Tech., 13, 6877–6887, doi:10.5194/amt-13-6877-2020, 2020.

Hare, J. S., Wilmouth, D. M., Smith, J. B., Klobas, J. E., Toohey, D. W., Hannun, R. A., Pittman, J. V., and Anderson, J. G.: Method for the production of a compact source of atomic line spectra in the vacuum ultraviolet, Appl. Optics, 63, 3685–3694, doi:10.1364/AO.520905, 2024.

Homeyer, C. R., and Bowman, K. P.: A 22-year evaluation of convection reaching the stratosphere over the United States, J. Geophys. Res. Atmos., 126, e2021JD034808, doi:10.1029/2021JD034808, 2021.

Homeyer, C. R., Smith, J. B., Bedka, K. M., Bowman, K. P., Wilmouth, D. M., Ueyama, R., Dean-Day, J. M., St. Clair, J. M., Hannun, R., Hare, J., Pandey, A., Sayres, D. S., Hanisco, T. F., Gordon, A. E., and Tinney, E. N.: Extreme altitudes of stratospheric hydration by midlatitude convection observed during the DCOTSS field campaign, Geophys. Res. Lett., 50, e2023GL104914, doi:10.1029/2023GL104914, 2023.

Homeyer, C. R., Gordon, A. E., Smith, J. B., Ueyama, R., Wilmouth, D. M., Sayres, D. S., Hare, J., Pandey, A., Hanisco, T. F., Dean-Day, J. M., Hannun, R., and St. Clair, J. M.: Stratospheric hydration processes in tropopause-overshooting convection revealed by tracer-tracer correlations from the DCOTSS field campaign, J. Geophys. Res. Atmos., 129, e2024JD041340, doi:10.1029/2024JD041340, 2024.

Howar, L. V., Salawitch, R. J., Wilmouth, D. M., Hintsa, E. J., Hare, J. S., Hanisco, T. F., St. Clair, J. M., Delaria, E. R., Atlas, E. L., Schauffler, S., Smith, K. R., Smith, J. B., Hall, B. D., Moore, F. L., Pittman, J. V., Daube, B., Bui, T. P., Li, Y., Keutsch, F. N., Sayres, D. S., Wofsy, S. C., Dean-Day, J., Donnelly, S., Treadway, V. A., Anderson, J. G., Homeyer, C. R., and Bowman, K. P.: Conditions necessary for chlorine activation in the midlatitude summer lower stratosphere, J. Geophys. Res. Atmos., 130, e2025JD043786, doi:10.1029/2025JD043786, 2025.

https://doi.org/10.5194/egusphere-2026-3480
Preprint. Discussion started: 25 June 2026

Hudson, P. K., Murphy, D. M., Cziczo, D. J., Thomson, D. S., de Gouw, J. A., Warneke, C., Holloway, J., Jost, H.-J., and Hübler, G.: Biomass-burning particle measurements: Characteristic composition and chemical processing, J. Geophys. Res., 109, D23S27, doi:10.1029/2003JD004398, 2004.

Jacquot, J. L., Shen, X., Abou-Ghanem, M., Froyd, K. D., Lawler, M., Schill, G. P., Slovacek, K., Thomson, D. S., Cziczo, D. J., and Murphy, D. M.: A new airborne single particle mass spectrometer: PALMS-NG, Aerosol Sci. Technol., 58, 991–1007, doi:10.1080/02786826.2024.2331549, 2024.

Jurkat, T., Voigt, C., Kaufmann, S., Zahn, A., Sprenger, M., Hoor, P., Bozem, H., Müller, S., Dörnbrack, A., Schlager, H., Bönisch, H., Engel, A.: A quantitative analysis of stratospheric HCl, HNO_3, and O_3 in the tropopause region near the subtropical jet, Geophys. Res. Lett., 41, 3315–3321, doi:10.1002/2013GL059159, 2014.

Kawa, S. R., Fahey, D. W., Heidt, L. E., Pollock W. H., Solomon S., Anderson, D. E., Loewenstein, M., Proffitt, M. H., Margitan, J. J., and Chan, K. R.: Photochemical partitioning of the reactive nitrogen and chlorine reservoirs in the high-latitude stratosphere, J. Geophys. Res., 97, 7905–7923, doi:10.1029/91JD02399, 1992.

Keim, E. R., Fahey, D. W., Del Negro, L. A., Woodbridge, E. L., Gao, R. S., Wennberg, P. O., Cohen, R. C., Stimpfle, R. M., Kelly, K. K., Hintsa, E. J., Wilson, J. C., Jonsson, H. H., Dye, J. E., Baumgardner, D., Kawa, S. R., Salawitch, R. J., Proffitt, M. H., Loewenstein, M., Podolske, J. R., and Chan K. R.: Observations of large reductions in the NO/NO_y ratio near the mid-latitude tropopause and the role of heterogeneous chemistry, Geophys. Res. Lett., 23, 3223–3226, doi:10.1029/96GL02593, 1996.

Khaykin, S., Legras, B., Bucci, S., Sellitto, P., Isaksen, L., Tencé, F., Bekki, S., Bourassa, A., Rieger, L., Zawada, D., Jumelet, J., and Godin-Beekman, S.: The 2019/20 Australian wildfires generated a persistent smoke-charged vortex rising up to 35 km altitude, Commun. Earth Environ., 1, 22, doi:10.1038/s43247-020-00022-5, 2020.

Liu, N., Liu, C., and Hayden, L.: Climatology and detection of overshooting convection from 4 years of GPM precipitation radar and passive microwave observations, J. Geophys. Res. Atmos., 125, e2019JD032003, doi:10.1029/2019JD032003, 2020.

Livesey, N. J., Read, W. G., Wagner, P. A., Froidevaux, L., Santee, M. L., Schwartz, M. J., Lambert, A., Millán, L. F., Pumphrey, H. C., Manney, G. L., Fuller, R. A., Jarnot, R. F., Knosp, B. W., and Lay, R. R.: Aura Microwave Limb Sounder (MLS) Version 5.0x Level 2 and 3 Data Quality and Description Document, JPL D-105336 Rev. B, Jet Propulsion Laboratory, https://mls.jpl.nasa.gov/data/v5-0_data_quality_document.pdf, 2022.

Ma, C., Su, H., Lelieveld, J., Randel, W., Yu, P., Andreae, M. O., and Cheng, Y.: Smoke-charged vortex doubles hemispheric aerosol in the middle stratosphere and buffers ozone depletion, Sci. Adv., 10, eadn3657, doi:10.1126/sciadv.adn3657, 2024.

Marcy, T. P., Fahey, D. W., Gao, R. S., Popp, P. J., Richard, E. C., Thompson, T. L., Rosenlof, K. H., Ray, E. A., Salawitch, R. J., Atherton, C. S., Bergmann, D. J., Ridley, B. A., Weinheimer, A. J., Loewenstein, M., Weinstock, E. M., and Mahoney, M. J.: Quantifying stratospheric ozone in the upper troposphere with in situ measurements of HCl, Science, 304, 261–265, doi:10.1126/science.1093418, 2004.

Marcy, T. P., Popp, P. J., Gao, R. S., Fahey, D. W., Ray, E. A., Richard, E. C., Thompson, T. L., Atlas, E. L., Loewenstein M., Wofsy, S. C., Park, S., Weinstock, E. M., Swartz, W. H., and Mahoney, M. J.: Measurements of

https://doi.org/10.5194/egusphere-2026-3480
Preprint. Discussion started: 25 June 2026

trace gases in the tropical tropopause layer, Atmos. Environ., 41, 7253–7261, doi:10.1016/j.atmosenv.2007.05.032, 2007.

Millán, L., Santee, M. L., Lambert, A., Livesey, N. J., Werner, F., Schwartz, M. J., Pumphrey, H. C., Manney, G. L., Wang, Y., Su, H., Wu, L., Read, W. G., and Froidevaux, L.: The Hunga Tonga-Hunga Ha'apai hydration of the stratosphere, Geophys. Res. Lett., 49, e2022GL099381, doi:10.1029/2022GL099381, 2022.

Murphy, D. M., Abou-Ghanem, M., Cziczo, D. J., Froyd, K. D., Jacquot, J., Lawler, M. J., Maloney, C., Plane, J. M. C., Ross, M. N., Schill, G. P., and Shen, X.: Metals from spacecraft reentry in stratospheric aerosol particles, Proc. Natl. Acad. Sci. U.S.A., 120, e2313374120, doi:10.1073/pnas.2313374120, 2023.

NASA/LARC/SD/ASDC: Dynamics and Chemistry of the Summer Stratosphere airborne data products [Dataset], NASA Langley Atmospheric Science Data Center Distributed Active Archive Center, doi:10.5067/ASDC/DCOTSS-Aircraft-Data_1, 2022.

Østerstrøm, F. F., Santee, M. L., Chipperfield, M. P., Evan, S., Smale, D., Wargan, K., Wilmouth, D. M., and Wohltmann, I.: Effects of the Hunga eruption on stratospheric ozone and related trace gases, in: APARC, 2025: The Hunga Eruption Atmospheric Impacts Report, edited by: Zhu, Y., Mann, G., Newman, P. A., and Randel, W., APARC Report No. 11, WCRP Report No. 10/2025, 107–136, doi:10.34734/FZJ-2025-05242, available at https://aparc-climate.org/publications/aparc-report-no-11/, 2025.

Plumb, R. A. and Ko, M. K. W.: Interrelationships between mixing ratios of long-lived stratospheric constituents, J. Geophys. Res., 97, 10145, doi:10.1029/92JD00450, 1992.

Revell, L. E., Bannister, M. T., Brown, T. F. M., Sukhodolov, T., Vattioni, S., Dykema, J., Frame, D. J., Cater, J., Chiodo, G., and Rozanov, E.: Near-future rocket launches could slow ozone recovery, npj Clim. Atmos. Sci., 8, 212, doi:10.1038/s41612-025-01098-6, 2025.

Robrecht, S., Vogel, B., Grooß, J.-U., Rosenlof, K., Thornberry, T., Rollins, A., Krämer, M., Christensen, L., and Müller, R.: Mechanism of ozone loss under enhanced water vapour conditions in the mid-latitude stratosphere in summer, Atmos. Chem. Phys., 19, 5805–5833, doi:10.5194/acp-19-5805-2019, 2019.

Salawitch, R. J., Wofsy, S. C., Wennberg, P. O., Cohen, R. C., Anderson, J. G., Fahey, D. W., Gao, R. S., Keim, E. R., Woodbridge, E. L., Stimpfle, R. M., Koplow, J. P., Kohn, D. W., Webster, C. R., May, R. D., Pfister, L., Gottlieb, E. W., Michelsen, H. A., Yue, G. K., Wilson, J. C., Brock, C. A., Jonsson. H. H., Dye, J. E., Baumgardner, D., Proffitt, M. H., Loewenstein, M., Podolske, J. R., Elkins, J. W., Dutton, G. S., Hintsa, E. J., Dessler, A. E., Weinstock, E. M., Kelly, K. K., Boering, K. A., Daube, B. C., Chan, K. R., and Bowen, S. W.: The distribution of hydrogen, nitrogen, and chlorine radicals in the lower stratosphere: implications for changes in O3 due to emission of NO_y from supersonic aircraft. Geophys. Res. Lett., 21, 2547–2550, doi:10.1029/94GL02781, 1994.

Salawitch, R. J. and McBride, L. A.: Australian wildfires depleted the ozone layer, Science, 378, 829–830, doi:10.1126/science.add2056, 2022.

Salawitch, R. J., Smith, J. B., Selkirk, H., Wargan, K., Chipperfield, M. P., Hossaini, R., Levelt, P. F., Livesey, N. J., McBride, L.A., Millán, L. F., Moyer, E., Santee, M. L., Schoeberl, M. R., Solomon, S., Stone, K., and Worden, H. M.: The imminent data desert: The future of stratospheric monitoring in a rapidly changing world, Bull. Amer. Meteor. Soc., 106, E540–E563, doi:10.1175/BAMS-D-23-0281.1, 2025.

https://doi.org/10.5194/egusphere-2026-3480
Preprint. Discussion started: 25 June 2026

Santee M. L., Lambert, A., Manney, G. L., Livesey, N. J., Froidevaux, L., Neu, J. L., Schwartz, M. J., Millán, L. F., Werner, F., Read, W. G., Park, M., Fuller, R. A. and Ward, B. M.: Prolonged and pervasive perturbations in the composition of the Southern Hemisphere midlatitude lower stratosphere from the Australian New Year's fires, Geophys. Res. Lett., 49, e2021GL096270, doi:10.1029/2021GL096270, 2022.

Santee, M. L., Lambert, A., Froidevaux, L., Manney, G. L., Schwartz, M. J., Millán, L. F., Livesey, N. J., Read, W. G., Werner, F., and Fuller, R. A.: Strong evidence of heterogeneous processing on stratospheric sulfate aerosol in the extrapolar Southern Hemisphere following the 2022 Hunga Tonga-Hunga Ha'apai eruption, J. Geophys. Res. Atmos., 128, e2023JD039169, doi:10.1029/2023JD039169, 2023.

Sargent, M. R., Sayres, D. S., Smith, J. B., Witinski, M., Allen, N. T., Demusz, J. N., Rivero, M., Tuozzolo, C., and Anderson, J. G.: A new direct absorption tunable diode laser spectrometer for high precision measurement of water vapor in the upper troposphere and lower stratosphere, Rev. Sci. Instrum., 84, 074102, doi:10.1063/1.4815828, 2013.

Sayres, D. S., Smith, J. B., Wilmouth, D. M., Pandey, A., Homeyer, C. R., Bowman, K. P., and Anderson, J. G.: Using the NAMA as a natural integrator to quantify the convective contribution to lower stratospheric water vapor over North America, J. Geophys. Res. Atmos., 129, e2024JD041641, doi:10.1029/2024JD041641, 2024.

Scott, S. G., Bui, T. P., Chan, K. R., and Bowen, S. W.: The meteorological measurement system on the NASA ER-2 aircraft, J. Atmos. Ocean. Tech., 7, 525–540, doi:10.1175/1520-0426(1990)007<0525:tmmsot>2.0.co;2, 1990.

Sharpe, S., Li, Y., Benjemia, S., Rivera-Adnorno, F., Olayemi, T., Ese, J., Shen, X., Fraund, M., Moffet, R., Lata, N. N., Cheng, Z., China, S., Homeyer, C. R., Dykema, J., Marcus, M. A., Wang, J., Cziczo, D., Keutsch, F., and Laskin, A.: Chemical imaging of individual stratospheric particles sampled over North America, Environ. Sci.: Atmos., 6, 47–60, doi:10.1039/d5ea00127g, 2026.

Shen, X., Jacquot, J. L., Li, Y., Sharpe, S. A. L., Dykema, J. A., Schill, G. P., Bowman, K. P., Homeyer, C. R., Fraund, M., Moffet, R. C., Olayemi, T. E., Pittman, J. V., Rivera-Adorno, F. A., Murphy, D. M., Smith, J. B., Laskin, A., Keutsch, F. N., and Cziczo, D. J.: Stratospheric aerosol perturbation by tropospheric biomass burning and deep convection, Nat. Geosci., 18, 1109–1116, doi:10.1038/s41561-025-01821-1, 2025.

Smith, J. B., Wilmouth, D. M., Bedka, K. M., Bowman, K. P., Homeyer, C. R., Dykema, J. A., Sargent, M. R., Clapp, C. E., Leroy, S. S., Sayres, D. S., Dean-Day, J. M., Bui, T. P., and Anderson, J. G.: A case study of convectively sourced water vapor observed in the overworld stratosphere over the United States, J. Geophys. Res. Atmos., 122, 9529–9554, doi:10.1002/2017JD026831, 2017.

Smith, K., Atlas, E., Apel, E. C., Blake, D. R., Dutton, G., Hornbrook, R. S., Montzka, S., Mühle, J., Schauffler, S. Treadway, V.: Chloromethanes in the North American troposphere and lower stratosphere over the past two decades, Geophys. Res. Lett., 51, e2024GL108710, doi:/10.1029/2024GL108710, 2024.

Solomon, S., Stone, K., Yu, P., Murphy, D. M., Kinnison, D., Ravishankara, A. R., and Wang, P.: Chlorine activation and enhanced ozone depletion induced by wildfire aerosol, Nature, 615, 259–264, doi:10.1038/s41586-022-05683-0, 2023.

https://doi.org/10.5194/egusphere-2026-3480
Preprint. Discussion started: 25 June 2026

St. Clair, J. M., Swanson, A. K., Bailey, S. A., and Hanisco, T. F.: CAFE: A new, improved nonresonant laser-induced fluorescence instrument for airborne in situ measurement of formaldehyde, Atmos. Meas. Tech., 13, 4581–4590, doi:10.5194/amt-12-4581-2019, 2019.

Stimpfle, R. M., Cohen, R. C., Bonne, G. P., Voss, P. B., Perkins, K. K., Koch, L. C., Anderson, J. G., Salawitch, R. J., Lloyd, S. A., Gao, R. S., Del Negro, L. A., Keim, E. R., and Bui, T. P.: The coupling of $ClONO_2$, ClO, and NO_2 in the lower stratosphere from in situ observations using the NASA ER-2 aircraft, J. Geophys. Res., 104, 26705–26714, doi:/10.1029/1999JD900288, 1999.

Stimpfle, R. M., Wilmouth, D. M., Salawitch, R. J., and Anderson, J. G.: First measurements of ClOOCl in the stratosphere: the coupling of ClOOCl and ClO in the Arctic polar vortex, J. Geophys. Res., 109, D03301, doi:10.1029/2003JD003811, 2004.

Stone, K., Solomon, S., Yu, P., Murphy, D. M., Kinnison, D., and Guan, J.: Two-years of stratospheric chemistry perturbations from the 2019-2020 Australian wildfire smoke, Atmos. Chem. Phys., 25, 7683–7697, doi:10.5194/acp-25-7683-2025, 2025.

Strahan, S. E., Smale, D., Solomon, S., Taha, G., Damon, M. R., Steenrod, S. D., Jones, N., Liley, B., Querel, R., and Robinson, J.: Unexpected repartitioning of stratospheric inorganic chlorine after the 2020 Australian wildfires, Geophys. Res. Lett., 49, e2022GL098290, doi:10.1029/2022GL098290, 2022.

Thornton, B. F., Toohey, D. W., Avallone, L. M., Hallar, A. G., Harder, H., Martinez, M., Simpas, J. B., Brune, W. H., Koike, M., Kondo, Y., Takegawa, N., Anderson, B. E., and Avery, M. A.: Variability of active chlorine in the lowermost Arctic stratosphere, J. Geophys. Res., 110, D22304, doi:10.1029/2004JD005580, 2005.

Thornton, B. F., Toohey, D. W., Tuck, A. F., Elkins, J. W., Kelly, K. K., Hovde, S. J., Richard, E. C., Rosenlof, K. H., Thompson, T. L., Mahoney, M. J., and Wilson, J. C.: Chlorine activation near the midlatitude tropopause, J. Geophys. Res., 112, D18306, doi:10.1029/2006JD007640, 2007.

von Hobe, M., Grooß, J.-U., Günther, G., Konopka, P., Gensch, I., Krämer, M., Spelten, N., Afchine, A., Schiller, C., Ulanovsky, A., Sitnikov, N., Shur, G., Yushkov, V., Ravegnani, F., Cairo, F., Roiger, A., Voigt, C., Schlager, H., Weigel, R., Frey, W., Borrmann, S., Müller, R., and Stroh, F.: Evidence for heterogeneous chlorine activation in the tropical UTLS, Atmos. Chem. Phys., 11, 241–256, doi:10.5194/acp-11-241-2011, 2011.

Wilkerson, J., Sayres, D. S., Smith, J. B., Allen, N., Rivero, M., Greenberg, M., Martin, T., and Anderson, J. G.: In situ observations of stratospheric HCl using three-mirror integrated cavity output spectroscopy, Atmos. Meas. Tech., 14, 3597–3613, doi:10.5194/amt-14-3597-2021, 2021.

Wilmouth, D. M., Stimpfle, R. M., Anderson, J. G., Elkins, J. W., Hurst, D. F., Salawitch, R. J., and Lait, L. R.: Evolution of inorganic chlorine partitioning in the Arctic polar vortex, J. Geophys. Res., 111, D16308, doi:10.1029/2005JD006951, 2006.

Wilmouth, D. M., Hanisco, T. F., Stimpfle, R. M., and Anderson, J. G.: Chlorine-catalyzed ozone destruction: Cl atom production from ClOOCl photolysis, J. Phys. Chem. A, 113, 14099–14108, doi:10.1021/jp9053204, 2009.

Wilmouth, D. M., Østerstrøm, F. F., Smith, J. B., Anderson, J. G., and Salawitch, R. J.: Impact of the Hunga Tonga volcanic eruption on stratospheric composition, Proc. Natl. Acad. Sci. USA, 120, e2301994120, doi:10.1073/pnas.2301994120, 2023.